Inverse Kinetic Isotope Fractionation During Bacterial Nitrite Oxidation

Karen L. Casciotti

Marine Chemistry and Geochemistry Department, Woods Hole Oceanographic Institution,
Woods Hole, MA 02643 USA

Contact information:
kcasciotti@whoi.edu
508-289-3738 (phone)
508-457-2076 (fax)

FINAL DRAFT ACCEPTED BY GCA

DECEMBER 29, 2008

ABSTRACT

Natural abundance stable isotopes in nitrate (NO_3^-), nitrite (NO_2^-), and nitrous oxide (N_2O) have been used to better understand the cycling of nitrogen in marine and terrestrial environments. However, in order to extract the greatest information from the distributions of these isotopic species, the kinetic isotope effects for each of the relevant microbial reactions are needed. To date, kinetic isotope effects for nitrite oxidation and anaerobic ammonium oxidation (anammox) have not been reported. In this study, the nitrogen isotope effect was measured for microbial nitrite oxidation to nitrate. Nitrite oxidation is the second step in the nitrification process, and it plays a key role in the regeneration of nitrate in the ocean. Surprisingly, nitrite oxidation occurred with an inverse kinetic isotope effect, such that the residual nitrite became progressively depleted in ^{15}N as the reaction proceeded. Three potential explanations for this apparent inverse kinetic isotope effect were explored: 1) isotope exchange equilibrium between nitrite and nitrous acid prior to reaction, 2) reaction reversibility at the enzyme level, and 3) true inverse kinetic fractionation. Comparison of experimental data to *ab initio* calculations and theoretical predictions leads to the conclusion that the fractionation is most likely inverse at the enzyme level. Inverse kinetic isotope effects are rare, but the experimental observations reported here agree with kinetic isotope theory for this simple N-O bond-forming reaction. Nitrite oxidation is therefore fundamentally different from all other microbial processes in which N isotope fractionation has been studied. The unique kinetic isotope effect for nitrite oxidation should help to better identify its role in the cycling of nitrite in ocean suboxic zones, and other environments in which nitrite accumulates.

1. INTRODUCTION

1.1 Application of Isotopes to Nitrogen Biogeochemistry

Stable isotope ratio measurements of nitrogen (N)-containing molecules have long provided insights into the relative rates of biogeochemical processes comprising the global nitrogen cycle. The kinetic fractionation factors ($\alpha_k = {}^{14}k/{}^{15}k$) and isotope effects ($\varepsilon_k = (\alpha_k - 1)*1000$) for key microbial processes offer constraints on the mechanisms of enzymatic reactions and provide the basis for interpretation of natural abundance N isotopic distributions in nature. For example, the kinetic isotope effects for both nitrogen fixation and denitrification, which add and remove bioavailable N from the ocean have been used to estimate the relative rates of these fluxes and thus the residence time of fixed N in the ocean (BRANDES and DEVOL, 2002; DEUTSCH et al., 2004; ALTABET, 2007).

The kinetic isotope effect for nitrogen fixation is small (-2 to +2‰; Table 1), which leads to addition of bioavailable N to the ocean with a $\delta^{15}N$ value near its source value of 0‰. Other sources of N to the ocean from atmospheric deposition and continental runoff are also believed to be near 0‰, although this value is highly uncertain (BRANDES and DEVOL, 2002). The processes that remove bioavailable N from the ocean include denitrification and anammox in suboxic regions within the water column and marine sediments (recently reviewed by DALSGAARD et al., 2005; FRANCIS et al., 2007). If the ocean N budget is in steady state, N would be removed by these processes with a flux-weighted average $\delta^{15}N$ value near 0‰ (ALTABET, 2007; BRANDES and DEVOL, 2002; DEUTSCH et al., 2004; DEVOL et al., 2006). While the isotope effects for anammox are not known at this time, the isotope effects for water column (20-30‰) and sedimentary (~0‰) denitrification have been used to partition N_2 losses between the water column and sediments. The large isotope effect for water column denitrification is a strong

59 constraint on this partitioning and implies that water column denitrification represents a
60 relatively small proportion of the total N_2 flux (BRANDES and DEVOL, 2002; DEUTSCH et al.,
61 2004; SIGMAN et al., 2003).

62 The large fractionation factor for nitrate reduction (BARFORD et al., 1999; DELWICHE and
63 STEYN, 1970; GRANGER et al., 2006) also leads to ^{15}N enrichment of nitrate in ocean suboxic
64 zones (BRANDES et al., 1998; CLINE and KAPLAN, 1975; SIGMAN et al., 2005; SIGMAN et al.,
65 2003; VOSS et al., 2001). Recently, Casciotti and McIlvin (CASCIOTTI and MCILVIN, 2007)
66 reported $\delta^{15}N_{NO3}$ values up to +21.7‰ (and $\delta^{18}O_{NO3}$ values up to +19.0‰) in the suboxic zone of
67 the eastern tropical North Pacific (ETNP). With a large fractionation factor for nitrate reduction
68 to nitrite, it would be expected for NO_2^- to be depleted in ^{15}N relative to NO_3^-. However, $\delta^{15}N_{NO2}$
69 values within the suboxic zone were as low as –18.5‰ (CASCIOTTI and MCILVIN, 2007). The
70 difference in $\delta^{15}N$ between nitrate and nitrite ($\Delta\delta^{15}N = \delta^{15}N_{NO3} - \delta^{15}N_{NO2}$) ranged from +28.4 to
71 +35.0‰ within the suboxic zone, with maximal values near the top of the secondary nitrite
72 maximum. These differences in $\delta^{15}N$ are larger than expected from the fractionation factor for
73 nitrate reduction during denitrification (20-30‰; Table 1), particularly if there is concomitant
74 nitrite consumption that acts to increase $\delta^{15}N_{NO2}$. These data suggest that either the fractionation
75 factor for nitrate reduction in the water column is larger than previous estimates, with
76 confounding effects on isotope-based oceanic nitrogen budgets (above), or that co-occurring
77 processes act to increase $\Delta\delta^{15}N$. Such processes would need to decrease $\delta^{15}N_{NO2}$ values relative
78 to $\delta^{15}N_{NO3}$, or increase $\delta^{15}N_{NO3}$ values while causing a minimal increase in $\delta^{15}N_{NO2}$.

79 In the suboxic zone, nitrite can be produced by nitrate reduction (CODISPOTI and
80 CHRISTENSEN, 1985; CODISPOTI et al., 1986; CODISPOTI and RICHARDS, 1976) or possibly
81 ammonia-oxidation (LIPSCHULTZ et al., 1990; WARD et al., 1989). The isotope effects for these

processes range from +13-38‰ (Table 1), but would be expressed to differing degrees depending on the extent of reaction completion. Nitrite consumption may be due to numerous processes, such as nitrite reduction to nitric oxide (NO) by denitrifying bacteria, nitrite reduction to N_2 by anammox bacteria (DALSGAARD et al., 2003; HAMERSLEY et al., 2007; KUYPERS et al., 2005; KUYPERS et al., 2003), or nitrite oxidation to nitrate by nitrite oxidizing bacteria (ANDERSON et al., 1982; CASCIOTTI and MCILVIN, 2007; LIPSCHULTZ et al., 1990; SIGMAN et al., 2005). Nitrite reduction to NO has been shown to occur with a normal kinetic isotope effect ($^{15}\varepsilon_{k,NIR} \approx +15‰$; (BRYAN et al., 1983)), which would increase $\delta^{15}N_{NO2}$ relative to $\delta^{15}N_{NO3}$ and lead to low $\Delta\delta^{15}N$ values. In order to better interpret N (and O) isotopic distributions of nitrate and nitrite in suboxic zones, the isotope effects for anammox and nitrite oxidation are needed. In this study, the kinetic isotope effect for nitrite oxidation was determined for pure cultures of the marine nitrite-oxidizing bacterium *Nitrococcus mobilis.*

1.2. Isotopic Fractionation

The differential distribution of isotopes between chemical species or phases, known as isotopic fractionation, has been recognized for many decades and is the basis for many applications in geochemistry (BIGELEISEN, 1952; BIGELEISEN, 1965; BIGELEISEN and MAYER, 1947; UREY, 1947). Both equilibrium and kinetic isotope effects can lead to isotopic fractionation between phases or chemical species. The equilibrium fractionation factor, $\alpha_{eq} = (A_2/A_1)/(B_2/B_1)$, defines the isotope ratios that two species, 'A' and 'B', would have at equilibrium, where '1' and '2' refer to the light and heavy isotopes, respectively. Equilibrium fractionation arises primarily from differences in the zero point energies of the molecules undergoing isotopic exchange, leading to enrichment of the heavy isotopes in the more strongly

bonded form (BIGELEISEN and MAYER, 1947; SCHAUBLE et al., 2001). This can be shown using the molecular partition functions, which represent the distribution of the relevant molecules between their available rotational, translational, and vibrational energy states (UREY, 1947; BIGELEISEN and MAYER, 1947; RICHET et al., 1977).

Kinetic fractionation factors (α_k) arise from small differences in the rates at which isotopically substituted molecules react, and are often the focus of stable isotope applications in biochemistry. Kinetic fractionation factors are defined by the instantaneous change in the isotope ratio of the reaction product (R_{Pi}) at a given substrate isotope ratio (R_S): $\alpha_k = R_S/R_{Pi}$ (MARIOTTI et al., 1981; SCOTT et al., 2004). The kinetic fractionation factor is also often represented by the ratio of rate constants, assuming first order reaction kinetics apply: $\alpha_k = k_1/k_2$, where '1' and '2' refer to the light and heavy isotopes, respectively (BIGELEISEN and WOLFSBERG, 1958).

For a reversible reaction, the ratio of kinetic isotope effects for forward and reverse reactions is also related to the equilibrium isotope effect: $\alpha_{eq} = \alpha_{kf}/\alpha_{kr}$, where α_{kf} is the kinetic isotope effect for the forward reaction and α_{kr} is the kinetic isotope effect for the reverse reaction (O'LEARY, 1981). Given that the inherent fractionation factors α_{eq}, α_{kf}, and α_{kr} are constant, this relation should hold at all times. However, the expression of this equality in the isotope ratios of substrates and products only holds at equilibrium.

Kinetic fractionation factors can also be calculated from first principles using transition state theory, where the substrate is assumed to be in thermal equilibrium with the transition state of the reaction (BIGELEISEN, 1949; BIGELEISEN, 1952; BUDDENBAUM and SHINER, 1977). If the isotopically substituted species is more stably bonded in the substrate than in the transition state, then molecules containing the heavy isotope will react more slowly. This behavior is termed "normal" kinetic isotope fractionation, and typically occurs in bond-breaking reactions. On the

other hand, if the isotopically substituted species is more stably bonded in the transition state, which may be the case in some bond-forming reactions, then molecules containing the heavy isotope may react more quickly. This phenomenon is referred to as "inverse" kinetic isotope fractionation, and may be expected to occur in some bond-forming reactions (FRY, 1970).

In this study, measurements of nitrate and nitrite $\delta^{15}N$ in pure culture experiments show that microbial nitrite oxidation occurs with an inverse kinetic isotope effect. Three potential mechanisms that could lead to this unusual fractionation are discussed: 1) a reversible reaction prior to the nitrite oxidation step ('pre-equilibrium'), 2) reversibility of the nitrite oxidation reaction itself ('enzyme reversibility'), and 3) a true enzyme-level inverse kinetic isotope effect. Examination of each of these mechanisms by comparison of experimental data to equilibrium and kinetic isotope fractionation theory suggests that this relatively simple bond-forming reaction proceeds with a true enzyme-level inverse kinetic isotope effect. Although inverse kinetic isotope effects are unusual in biochemistry, here I argue that its occurrence in nitrite oxidation should be expected and may have important implications for understanding marine nitrogen isotope biogeochemistry and nitrite cycling in suboxic zones.

2. MATERIALS AND METHODS

2.1 Growth and Maintenance of Bacterial Cultures

Nitrococcus mobilis, a marine nitrite-oxidizing bacterium (NOB) isolated from the Equatorial Pacific Ocean near the Galapagos Islands (WATSON and WATERBURY, 1971), was generously provided by Frederica Valois (Woods Hole Oceanographic Institution). *N. mobilis* is a member of the gamma-*Proteobacteria* that grows optimally at 25-30 °C and at pH 7.5-8.0 in 70-100% seawater (WATSON and WATERBURY, 1971). It is an obligate chemolithoautotroph, which fixes

carbon dioxide into biomass using NO_2^- as an electron source (WATSON and WATERBURY, 1971). In addition to oxidizing NO_2^- to NO_3^-, most nitrite oxidizing bacteria can assimilate NO_3^-, NO_2^-, and NH_4^+ during growth (STARKENBURG et al., 2006). The physiology of *N. mobilis* has not been studied exhaustively, but its draft genome contains genes required to transport nitrite, assimilate nitrite (*nirB*), and reduce nitrite to nitric oxide (*nirK*). No genes have been found in this organism for ammonium oxidation to nitrite.

In this study, *N. mobilis* was maintained in marine NOB medium containing 75% seawater and 25% distilled water amended with 400 μM $MgSO_4$, 30 μM $CaCl_2$, 5 μM K_2HPO_4, 2.3 μM Fe(III)-EDTA ("Geigy iron"), 0.1 μM Na_2MoO_4, 0.25 μM $MnCl_2$, 0.002 μM $CoCl_2$, and 0.08 μM $ZnSO_4$ (WATSON and WATERBURY, 1971). Filter-sterilized $NaNO_2$ was added to a final concentration of 10 mM after autoclaving the base medium. One-liter cultures were inoculated by transfer of 100 mL cultures (that had exhausted their NO_2^-) into 900 mL NOB medium. The one-liter maintenance cultures were then grown for approximately one month before transfer or experimentation.

2.2 Nitrite Oxidation Experiments

To collect *N. mobilis* cells for isotopic fractionation experiments, 300 mL of maintenance culture (cell density ~ 10^8 cells/mL) were harvested by centrifugation at 7600 g for 20 minutes in six 50 mL sterile centrifuge tubes. The cell pellets were each washed with 2 mL sterile marine NOB medium containing 100 μM $NaNO_2$. Washed cells were pooled, then re-aliquotted into sterile 2 mL centrifuge tubes and collected by centrifugation at 10,000 g. The supernatant was pipetted away and the cells were resuspended and pooled in 8 mL sterile marine NOB medium with 100 μM $NaNO_2$.

Results from three independent experiments are reported here. The first experiment (hereafter referred to as 'Experiment 1') was initiated by adding 0.5 mL of washed cells to flask "A" and 1.0 mL to flask "B", each containing 100 mL marine NOB medium with 100 μM $NaNO_2$ at pH 8.2. A third flask received no cells and was incubated with 100 μM NO_2^- as an uninoculated control. In the second experiment (hereafter referred to as 'Experiment 2'), nine 250 mL flasks were prepared, each with 100 mL of NOB medium at pH 7.8. Experiment 2 was initiated by adding 0.5 mL of washed cells to triplicate "A" flasks and 1.0 mL to triplicate "B" flasks. The three final flasks received no cells (uninoculated controls). In the third experiment (hereafter referred to as "Experiment 3'), three 250 mL flasks were prepared, each with 100 mL of medium with 100 μM $NaNO_2$ at pH 8.8. Experiment 3 was initiated by adding 0.5 mL of washed cell suspension to flask "A" and 1.0 mL to flask "B". The third flask received no cells and was incubated as an uninoculated control. In each experiment, final cell densities were estimated to be on the order of 10^6 -10^7 cells/mL, with half as many cells in "A" flasks compared with "B" flasks.

Flasks were incubated at room temperature with shaking (Experiments 1 and 2) or without shaking (Experiment 3). Time course samples were collected immediately after inoculation and periodically thereafter until approximately all of the NO_2^- had been converted to NO_3^- (2-6 days, depending on the experiment). At each time point, 10-15 mL were withdrawn for nitrite and nitrate concentration analyses, as well as for nitrite and nitrate isotopic analyses; these samples were passed through a 0.2 μM pore size membrane filter and stored frozen.

195 **2.3 Chemical Analyses**

196 NO_2^- concentrations were analyzed in duplicate using the Greiss-Islovay colorimetric
197 reaction (STRICKLAND and PARSONS, 1972). Combined NO_2^-+NO_3^- concentrations were
198 determined from the m/z = 44 peak area obtained by isotopic analyses using the denitrifier
199 method (SIGMAN et al., 2001; CASCIOTTI et al., 2002). A two-point calibration for NO_2^-+NO_3^-
200 concentration was derived from blank (0 μM added) and 20 μM standards, analyzed after every
201 nine samples. Most samples were analyzed in duplicate, and uncertainties in [NO_2^-+NO_3^-] were
202 derived from replicate analyses where possible. NO_3^- concentrations were calculated by
203 difference between [NO_2^-+NO_3^-] and [NO_2^-], and standard deviations for [NO_3^-] measurements
204 were calculated by error propagation from standard deviations of [NO_2^-] and [NO_2^-+NO_3^-]
205 measurements.

206

207 **2.4 Isotopic Analyses and Corrections**

208 Nitrite $\delta^{15}N$ values ($\delta^{15}N_{NO2} = ([^{15}N/^{14}N]_{NO2}/[^{15}N/^{14}N]_{AIR} - 1)\times 1000$) from the time course
209 samples were analyzed by reaction with acetic acid-buffered sodium azide to form nitrous oxide
210 (N_2O) via the "azide method" (MCILVIN and ALTABET, 2005). Isotope ratios of the produced
211 N_2O were measured by continuous flow isotope ratio mass spectrometry (CF-IRMS) using an
212 on-line purge and trap system for extraction and purification of the N_2O analyte (see CASCIOTTI
213 et al., 2007). Analyses were calibrated to the AIR-N_2 reference scale using sodium nitrite salts
214 with calibrated $\delta^{15}N_{NO2}$ values: N-23 (+3.7‰), N-7373 (-79.6‰), and N-10219 (+2.5‰)
215 (CASCIOTTI et al., 2007). Solutions of these standard nitrite materials were reacted and analyzed
216 in parallel to nitrite samples, with an aliquot of each standard analyzed initially and after every
217 nine experimental samples. Sample and standard quantities were matched to achieve 10 nmoles

of either sample or standard NO_2^- converted to 10 nmoles of N_2O by reaction with sodium azide. In this technique, one nitrogen atom in the N_2O arises from NO_2^- and one from azide (McIlvin and Altabet, 2005). Analyses were conducted only on samples with NO_2^- concentrations greater than 1 μM. Each sample was analyzed in duplicate and the $\delta^{15}N$ values are reported as the average ± one standard deviation.

Nitrate plus nitrite $\delta^{15}N$ values ($\delta^{15}N_{NO2+NO3} = ([^{15}N/^{14}N]_{NO2+NO3}/[^{15}N/^{14}N]_{AIR} - 1)\times 1000$) were analyzed by bacterial conversion of nitrogen oxides (NO_2^- and NO_3^-) to N_2O via the "denitrifier method" (Casciotti et al., 2002; Sigman et al., 2001). The isotopes of N_2O were analyzed via CF-IRMS, as described above. Analyses were calibrated to the AIR-N_2 reference scale using potassium nitrate reference materials USGS32 ($\delta^{15}N$ = +180.0‰), USGS34 ($\delta^{15}N$ = -1.8‰), and USGS35 ($\delta^{15}N$ = +2.7‰) (Bohlke et al., 2003). Standards were reacted and analyzed in parallel to samples, with an aliquot of each standard analyzed initially and after every nine experimental samples. Sample and standard quantities were matched to achieve 20 nmoles of sample ($NO_2^- + NO_3^-$) or standard (NO_3^-) converted to 10 nmoles N_2O by the denitrifier method. Most samples were analyzed in duplicate and are reported as average values ± one standard deviation.

The majority of the time course samples contained a mixture of NO_2^- and NO_3^-. Therefore, in order to estimate nitrate $\delta^{15}N$ ($\delta^{15}N_{NO3}$) values, the procedure previously described (Casciotti and McIlvin, 2007) was followed for mass and isotope balance of the mixture components: $\delta^{15}N_{NO3} = (\delta^{15}N_{NO2+NO3} \times [NO_2^- + NO_3^-] - \delta^{15}N_{NO2} \times [NO_2^-]) \div [NO_3^-]$. The approximation required by this equation that ^{15}N is a minor constituent does not introduce significant error in $\delta^{15}N_{NO3}$ estimation for the samples described here. Standard deviations for $\delta^{15}N_{NO3}$ were calculated by error propagation using the standard deviations for $\delta^{15}N_{NO2}$, $\delta^{15}N_{NO2+NO3}$, and

241 concentration measurements. For samples with a single $\delta^{15}N_{NO2+NO3}$ analysis, the standard
242 deviation was assumed to be 0.3‰ (SIGMAN et al., 2001).
243
244 **2.5 Fractionation Factor Estimates**
245 The kinetic fractionation factor for nitrite oxidation ($^{15}\alpha_{k,NXR}$) was calculated from the
246 $\delta^{15}N_{NO2}$ data using a closed-system Rayleigh distillation model (SCOTT et al., 2004): $\ln(^{15}R_{NO2})$
247 $= (1/^{15}\alpha_{k,NXR} - 1)\cdot\ln(C) + \ln(^{15}R_{NO2,0}/C_0^{(1/\alpha,kNXR-1)})$, where $^{15}R_{NO2}$ is the $^{15}N/^{14}N$ ratio of NO_2^-
248 (unitless) and $^{15}R_{NO2,0}$ is its initial value. C is the NO_2^- concentration (μM) and C_0 is its initial
249 value. $^{15}\alpha_{k,NXR}$ (unitless) is the ratio of the first order rate constants for $^{14}NO_2^-$ and $^{15}NO_2^-$
250 oxidation, respectively ($^{14}k_{NXR}/^{15}k_{NXR}$). Fractionation factors calculated in this way are the
251 reciprocal of those discussed by Mariotti et al (MARIOTTI et al., 1981).
252 Dummy variables were used to obtain the average and standard deviation of $^{15}\alpha_{k,NXR}$ for all
253 experiments (SCOTT et al., 2004). This procedure utilizes the equation $y = \beta x + \gamma_1 + \gamma_2 D_2 + \gamma_3$
254 D_3, where $y = \ln(^{15}R_{NO2})$, $x = \ln(C)$, and $\beta = (1/^{15}\alpha_{k,NXR} - 1)$. First, experimental data were
255 combined from different flasks to obtain the y-intercept for experiment 1 (γ_1) and the y-intercept
256 offset from γ_1 for experiments 2 (γ_2) and 3 (γ_3). Cell density did not appreciably change the
257 observed kinetic isotope effect, so "A" and "B" flasks from each experiment were treated as
258 replicates for this purpose. Next, the β value was determined from each x-y pair, and the $^{15}\alpha_{k,NXR}$
259 value was calculated from each β value. Finally, the average and standard deviation for $^{15}\alpha_{k,NXR}$
260 were calculated from the entire dataset.
261

2.6 Ab Initio Calculations of Molecular Vibration Frequencies

Molecular vibration frequencies for two isotopic forms (containing either ^{15}N or ^{14}N) of NO_2^-, HNO_2, and NO_3^- were calculated using the Gaussian interface through the WebMO (Version 8.0.011e) guest server at buchner.chem.hope.edu. The geometry of each molecule was first optimized in either 'water' or 'no solvent', depending on the desired phase of the vibration calculations. The optimized molecules were then used to calculate the molecular vibration frequencies using B3LYP density function theory with the 'routine' basis set (6-31G(d)) (ANBAR et al., 2005) in both 'no solvent' and in aqueous solution. The geometry optimization and vibration calculations were performed three times each, and the frequencies obtained varied by less than 0.01%.

3. RESULTS

3.1 Time Course Experiments

In each independent experiment, NO_2^- was oxidized to NO_3^- by pure cultures of *N. mobilis* over a course of 2-6 days (Figure 1A, C, E). NO_2^- removal was nearly complete in each inoculated flask. Each experiment was conducted using a two-fold range of cell densities (approximately 2-4 x 10^7 cells mL^{-1}), depending on the volume of concentrated cell suspension added. The net rate of nitrite oxidation apparently increased with cell density (Figure 1A, C, E). For the most part, mass balance was maintained between NO_2^- and NO_3^- pools as NO_2^- was consumed. Concentrations of $NO_2^-+NO_3^-$ in experimental flasks showed up to 10-20% variation at some time points, but as discussed below, there was no change in $\delta^{15}N_{NO2+NO3}$ corresponding to these apparent changes in $[NO_2^-+NO_3^-]$. Control flasks also showed similar variability in $[NO_2^-+NO_3^-]$, suggesting that the variability was most likely not biological in nature. At this

285 time, the most likely explanation is error in concentration measurement at particular time points
286 in the time course.

287 In every case, the nitrite became progressively depleted in ^{15}N, decreasing from initial $\delta^{15}N$
288 values of +0.7‰ to less than –50‰ as it was oxidized to NO_3^- (Figure 1B, D, F). In contrast,
289 uninoculated control flasks showed no change $\delta^{15}N_{NO2}$ values over the time course. Control
290 flasks also showed no change in the $\delta^{18}O$ value of $NO_2^-+NO_3^-$ (data not shown), a measurement
291 that is very sensitive to changes in the fractions of nitrate and nitrite in the mixture (CASCIOTTI et
292 al., 2007). Finally, within the standard error of the measurement (~0.3‰) $\delta^{15}N_{NO2+NO3}$ did not
293 change over the time course in any flask, whether nitrite oxidation occurred (experimental flasks)
294 or not (control flasks) (Figure 1 B, D, F). The consistency of $\delta^{15}N_{NO2+NO3}$ over the time course is
295 a strong constraint on mass balance between NO_2^- and NO_3^- because any potential loss of N from
296 the NO_2^- and NO_3^- pools would have needed to possess a constant $\delta^{15}N$ value of +1‰, even as
297 $\delta^{15}N_{NO2}$ decreased from +1‰ to -52‰. Isotopically, it would be difficult to account for los of
298 NO_2^- to other pools of N that were not measured (cell biomass, NO, NH_4^+).

299 Mass balance allows the calculation of the $\delta^{15}N$ of accumulated NO_3^- over the time course
300 (CASCIOTTI and MCILVIN, 2007). As expected from a closed-system isotope mass balance,
301 $\delta^{15}N_{NO3}$ was highest initially, then decreased over the time course to a value within error of the
302 initial $\delta^{15}N_{NO2}$ (not shown). The maintenance of mass (Figure 1A, C, E) and isotope (Figure 1B,
303 D, F) balance between nitrate and nitrite in experimental flasks and the lack of nitrite oxidation
304 to nitrate in control flasks points towards biological nitrite oxidation as the process responsible
305 for NO_2^- consumption in these experiments.
306

3.2 Rayleigh Fractionation

Analysis of the observed trends in $\delta^{15}N_{NO2}$ using a closed system Rayleigh model yields estimates for $^{15}\alpha_{k,NXR}$ of 0.9873 ± 0.0010, 0.9867 ± 0.0018, and 0.9882 ± 0.0005 for the three experiments, respectively (Figure 2). Averaging over all experiments yields an estimate of 0.9872 ± 0.0015 for $^{15}\alpha_{k,NXR}$. In all three experiments, the kinetic fractionation factor appears to be inverse. In addition, the three experiments were all very similar to each other, with individual estimates for $^{15}\alpha_{k,NXR}$ within two standard deviations of the overall $^{15}\alpha_{k,NXR}$.

As observed in Figure 2, the fractionation factor appeared to increase slightly (become less inverse) after approximately 80% of the nitrite has been oxidized, as indicated by the deviation from the $^{15}\alpha_{k,NXR} = 0.9872$ line at $\ln([NO_2^-])$ values below 2 (corresponding to $[NO_2^-]$ less than ~7 μM) (Figure 2). Both experiments 1 and 2 showed this change of slope. Inclusion of these points in the analysis may be one reason for the slight variation between $^{15}\alpha_{k,NXR}$ in experiments 1, 2, and 3. The apparent change in $^{15}\alpha_{k,NXR}$ at later time points in the experiment may result from departures of the system from the basic assumption of a unidirectional closed system inherent in the Rayleigh distillation equation. Many systems show a tendency towards smaller isotope effects at high extents of substrate consumption as a result of diffusive limitation or active transport of substrate (FARQUHAR et al., 1982; GRANGER et al., 2008; GRANGER et al., 2006; NEEDOBA et al., 2004; O'LEARY, 1981). Given that the *N. mobilis* experiments were conducted with whole cells, these factors may play a role in the expressed isotope effect, which I will return to below. However, both diffusion of NO_2^- and uptake by the cell are likely to have small, normal kinetic isotope effects (GRANGER et al., 2008; WASER et al., 1998b), and are likely to be of secondary importance in the current analysis.

4. DISCUSSION

Given that true inverse kinetic isotope effects are rare, two alternative explanations were considered for the observed results. First, one must consider whether nitrite with low $\delta^{15}N$ could have been produced in the experiments over time, thus mimicking an inverse kinetic isotope effect. The only mechanism possible for nitrite production in *N. mobilis* is through reduction of nitrate by reversible reaction of the nitrite oxidoreductase enzyme. The membrane-bound nitrite oxidoreductase enzymes isolated from *Nitrobacter agilis* and *Nitrobacter hamburgensis* have been shown to be reversible under low pH (TANAKA et al., 1983) and reducing conditions (MEINCKE et al., 1992; SUNDERMEYER-KLINGER et al., 1984). Although oxygen concentrations are not expected to have been limiting in the current *N. mobilis* experiments, enzyme-level reversibility is one mechanism that could produce an apparent inverse kinetic isotope effect, if the reverse reaction (nitrate reduction) is more highly fractionating than the forward reaction (nitrite oxidation). Therefore, the possibility for enzymatic back-reaction of NO_3^- to NO_2^- was carefully examined in section 4.1.2.

The second scenario under which a normal enzyme-level kinetic fractionation factor may appear to be inverse involves equilibrium between the true substrate for the reaction and a larger pool of non-reactive substrate. This is termed a "pre-equilibrium" scenario because the equilibrium reaction would occur prior to the enzymatic reaction, rather than at the enzyme level. For example, a pH-dependent pre-equilibrium between H_2S and HS^- was used to explain the small inverse kinetic isotope effect observed in anaerobic sulfide oxidation (FRY et al., 1984). The pH-dependent isotope exchange between NO_2^- and HNO_2 is examined here in section 4.1.1. Rejecting these two scenarios, in which the apparent inverse fractionation factor would be driven by equilibrium or reversibility, it is shown that transition state theory supports the observation of

353 an inverse kinetic fractionation factor for nitrite oxidoreductase at the enzyme level (Section
354 4.1.3).
355
356 **4.1 Potential Explanations for the Inverse Isotope Effect**
357 *4.1.1 Pre-equilibrium*
358 Apparent inverse fractionation factors have been observed in systems where a fractionating
359 equilibrium reaction precedes a unidirectional enzymatic reaction. An example of this is in
360 anaerobic oxidation of sulfide to elemental sulfur (S^0) by the purple photosynthetic bacterium
361 *Chromatium vinosum* (FRY et al., 1984). An inverse isotope effect was observed, whereby the
362 sulfide undergoing oxidation became depleted ^{34}S over time. The S^0 produced by this reaction
363 was initially enriched in ^{34}S, but then also became depleted over time, approaching the $\delta^{34}S$ of
364 the initial substrate. However, in the sulfide oxidation reaction, the apparent inverse kinetic
365 isotope effect was explained by co-occurring equilibrium and kinetic isotope effects, rather than
366 a true inverse kinetic isotope effect (FRY et al., 1984). The equilibrium isotope effect between
367 hydrogen sulfide (H_2S) and bisulfide (HS^-) caused the substrate for the reaction, H_2S, to be
368 enriched in ^{34}S by approximately 6‰ relative to the HS^- (FRY et al., 1984). Therefore, when H_2S
369 reacted with a small *normal* kinetic isotope effect the overall process produced S^0 that was
370 enriched in ^{34}S relative to the total reduced sulfur pool, yielding an apparently inverse kinetic
371 isotope effect.
372 In the case of nitrite oxidation to nitrate, it is often assumed that the substrate for the reaction
373 is NO_2^-, although few experiments have been specifically designed to distinguish between HNO_2
374 and NO_2^- as substrates (BOON and LAUDELOUT, 1962). Given this uncertainty, the possibility that
375 HNO_2 could have a significantly different $\delta^{15}N$ from the total N(III) pool (NO_2^- + HNO_2) must

be considered. Nitrous acid (HNO_2) has a pKa of 2.8 (RIORDAN et al., 2005), and at pH 8 more than 99.999% of the total N(III) occurs in the form of NO_2^-, and less than 0.001% of the N(III) occurs in the form of HNO_2. In order for the pH-dependent pre-equilibrium to explain the observed inverse kinetic isotope effect, 1) the minor pool (in this case, HNO_2) must be the substrate for the reaction, 2) HNO_2 must be enriched in ^{15}N relative to NO_2^-, and 3) the magnitude of the equilibrium isotope effect must be large enough to overcome a normal enzyme-level kinetic isotope effect for the oxidation to nitrate. The scenarios that would allow the observed inverse isotope effect to be consistent with a normal enzyme-level kinetic isotope effect, were evaluated through *ab initio* calculation of the equilibrium isotope effect for N isotope exchange between HNO_2 and NO_2^-, in combination with six different Rayleigh model simulations (see below for additional details). .

The nitrogen isotope exchange between HNO_2 and NO_2^- is represented by equation (1):

$$H^{14}NO_2 + {}^{15}NO_2^- \xleftrightarrow{{}^{15}\alpha_{eq,HNO_2/NO_2}} H^{15}NO_2 + {}^{14}NO_2^- \quad (1)$$

where ${}^{15}\alpha_{eq,HNO2/NO2}$ is the fractionation factor for this isotope exchange equilibrium. As discussed earlier, ${}^{15}\alpha_{eq,HNO2/NO2}$ defines the ratio of isotope ratios of HNO_2 and NO_2^- at equilibrium $({}^{15}R_{HNO2}/{}^{15}R_{NO2})_{eq}$. This equilibrium fractionation factor can be calculated (with some approximations that are suitable for isotopes other than hydrogen) using the reduced partition functions (Q) if the vibration frequencies of the ^{14}N and ^{15}N-containing molecules of both species are known (UREY, 1947). Equation 2 illustrates how ${}^{15}\alpha_{eq,HNO2/NO2}$ is related to the reduced partition function ratios for the two species.

$$^{15}\alpha_{eq,HNO2/NO2} = \frac{^{15}Q_{HNO2}/^{14}Q_{HNO2}}{^{15}Q_{NO2}/^{14}Q_{NO2}} \quad (2)$$

Equation 3 shows how the reduced partition function ratio for either HNO_2 or NO_2^- is calculated from the normal mode molecular vibration frequencies of ^{15}N and ^{14}N-containing molecules.

$$\frac{Q_{15}}{Q_{14}} = \frac{\sigma_{14}}{\sigma_{15}} \prod_i \frac{u_{15i}}{u_{14i}} \cdot \frac{e^{-u_{15i}/2}}{e^{-u_{14i}/2}} \cdot \frac{1-e^{-u_{14i}}}{1-e^{-u_{15i}}} \quad (3)$$

In equation 3, Q_{14} and Q_{15} are the reduced partition function ratios relative to the separated atoms, for ^{14}N and ^{15}N-containing molecules, respectively. σ_{14} and σ_{15} are the symmetry numbers for the two isotopically substituted species. In addition, $u_i = hc\omega_i/kT$, where ω_i corresponds to each of the i^{th} normal frequencies (bent polyatomic molecules with N atoms have 3N-6 normal frequencies), *h* is Plank's constant, *k* is Boltzman's constant, c is the speed of light, and T is the absolute temperature in K (here, T = 298 K). Therefore, in order to obtain a first-order estimate for $^{15}\alpha_{eq,HNO2/NO2}$, we need only the molecular vibration frequencies for $H^{14}NO_2$, $H^{15}NO_2$, $^{14}NO_2^-$, and $^{15}NO_2^-$. For additional discussion of the assumptions and simplifications involved in using equations 2 and 3, please see Bigeleisen and Mayer (1947) and Urey (1947).

A collection of observed (BEGUN and FLETCHER, 1960; DEELEY and MILLS, 1985) and calculated (*this study*) vibration frequencies for NO_2^- and HNO_2 are given in Table 2. Aqueous vibration frequencies were available for NO_2^- and NO_3^- (BEGUN and FLETCHER, 1960), but not for HNO_2. For HNO_2 the only available vibration frequencies were in gas phase (DEELEY and MILLS, 1985). Given that the molecular vibrations could be quite different in aqueous vs. gas phase (RICHET et al., 1977), vibrational frequencies were needed for HNO_2 in the aqueous phase.

To check the accuracy of the calculation, the aqueous phase vibration frequencies for NO_2^- and gas phase vibration frequencies for HNO_2 were also calculated to compare with observed frequencies (Table 2). Finally, to test the sensitivity to solvation the vibration frequencies for NO_2^- were also calculated for the 'no solvent' case.

The calculated frequencies for NO_2^- and HNO_2 were similar to observed frequencies, with differences ranging from -6.8 to +1.5% for ^{14}N-containing species and -6.7 to +1.7% for ^{15}N-containing species (Table 2). The frequency shifts upon isotopic substitution were also similar. On average, a 1.13% vibrational frequency shift upon substitution with ^{15}N was obtained in the calculated frequencies, compared with a 1.16% vibrational shift in the observed frequencies. Finally, the normal modes that appeared insensitive to isotopic substitution in the modeled frequencies also showed little isotopic shift in the observed frequencies. The comparison between modeled and observed frequencies gives some confidence in the calculated results, although both observed and calculated frequencies could be inaccurate for different reasons. The differences between calculated aqueous and gas phase frequencies were less than 2.5% in all cases.

The modeled frequencies were used to calculate the equilibrium fractionation factor for nitrogen exchange between NO_2^- and HNO_2 using equations 2 and 3. Little difference was obtained for $^{15}\alpha_{eq,HNO2/NO2}$ in aqueous (0.9975) versus gas (0.9972) phase (Table 3). In addition, use of the observed frequencies (from mixed phases) yields an $^{15}\alpha_{eq,HNO2/NO2}$ value of 0.9970, which is very similar to the $^{15}\alpha_{eq,HNO2/NO2}$ values obtained from the *ab initio* frequencies. In all cases, the calculated $^{15}\varepsilon_{eq,HNO2/NO2}$ values were small at room temperature (-3 to -2.5‰), and HNO_2 was predicted to be depleted in ^{15}N relative to NO_2^-. Given these results for HNO_2/NO_2^- equilibration, it is anticipated that HNO_2 would have been depleted in ^{15}N relative to NO_2^- by 2.5

444 to 3.0‰ in the *N. mobilis* experiments (room temperature, pH 7.8 - 8.8). In contrast to the
445 H_2S/HS^- equilibrium where protonation and deprotonation directly affect the bonding
446 environment of the sulfur atom (a primary isotope effect), protonation and deprotonation of NO_2^-
447 does not occur at the central N atom. Therefore, it is not surprising that protonation and
448 deprotonation of the NO_2^-/HNO_2 couple should exhibit a small isotope effect.
449 Given the small equilibrium isotope effect between HNO_2 and NO_2^-, it can be shown that
450 reaction of either NO_2^- or HNO_2 with a normal fractionation factor cannot explain an apparent
451 inverse kinetic fractionation factor of the magnitude that we observe. This is illustrated in detail
452 through Rayleigh simulations using various estimates for the kinetic (normal vs. inverse) and
453 equilibrium isotope effects, and using either HNO_2 or NO_2^- as substrate for the reaction
454 (*Electronic Annex* 1). The pre-equilibrium between HNO_2 and NO_2^- can therefore be rejected as
455 a mechanism contributing to the apparent inverse kinetic fractionation factor.
456
457 *4.1.2. Enzyme-Level Reversibility*
458 Enzyme reversibility could lead to an apparent inverse isotope effect, even if the forward and
459 reverse reactions are normal, if 1) the reverse reaction has a larger isotope effect than the forward
460 reaction, and 2) there is sufficient mass flux in the reverse reaction to lead to isotopic depletion
461 of the primary substrate pool. The flux required to obtain an apparent inverse isotope effect will
462 vary inversely with the magnitude of the isotope effect for the reverse reaction, in this case
463 nitrate reduction to nitrite.
464 Nitrite oxidoreductase is known to be reversible (SUNDERMEYER-KLINGER et al., 1984;
465 TANAKA et al., 1983). For example, some studies have shown growth of *Nitrobacter* under
466 anaerobic conditions using nitrate as a terminal electron acceptor (AHLERS et al., 1990; BOCK et

al., 1988; FREITAG and BOCK, 1990; FREITAG et al., 1987), and other studies have shown that *Nitrobacter* can assimilate nitrate-N (KUMAR and NICHOLAS, 1982). Both processes require a mechanism for reducing nitrate to nitrite; however, nitrate reductase has not been found in any of the nitrite oxidizer genomes studied thus far, including *Nitrococcus mobilis* (STARKENBURG et al., 2008). Instead, it is believed that nitrite oxidoreductase acts as the nitrate reductase under certain growth conditions. This theory is based on the biochemical similarity (YAMANAKA, 1996; YAMANAKA and FUKUMORI, 1988) and evolutionarily relatedness of the genes for nitrite oxidoreductase to the *narGH* family of dissimilatory nitrate reductases (STARKENBURG et al., 2008), as well as observed reversibility of partially purified nitrite oxidoreductase from *Nitrobacter* species (TANAKA et al., 1983; YAMANAKA and FUKUMORI, 1988). The biochemistry of nitrite oxidoreductase has not been studied in *Nitrococcus* species directly, but the nitrite oxidizing systems appear to be similar between the two genera (BARTOSCH et al., 1999; SPIECK and BOCK, 2001), and some reversibility of this enzyme might be expected under some circumstances.

Here the role of enzyme reversibility in the observed inverse kinetic isotope effect for nitrite oxidation was evaluated. Two aspects of this question are discussed: first, whether equilibrium calculations for the nitrite/nitrate redox system support a normal kinetic isotope effect for the forward reaction (nitrite oxidation to nitrate) and second, whether significant back reaction (nitrate reduction to nitrite) can be detected during experiments 1-3. To address the first component, the equilibrium fractionation factor for isotope exchange between nitrate and nitrite (equation 4) was first computed.

$$^{14}NO_2^- + {}^{15}NO_3^- \xleftrightarrow{{}^{15}\alpha_{eq,NO2/NO3}} {}^{15}NO_2^- + {}^{14}NO_3^- \quad (4)$$

The equilibrium fractionation factor for the isotope exchange reaction ($^{15}\alpha_{eq,NO2/NO3}$) can be calculated using the same principles as applied above to calculate the isotope effect for nitrogen isotope exchange between NO_2^- and HNO_2 (equations 2 and 3). Table 2 contains the relevant molecular vibration frequencies for NO_2^- and NO_3^- for use in equation 3. Using the calculated molecular vibrations for NO_2^- and NO_3^- in aqueous solution, it is estimated that $^{15}\alpha_{eq,NO2/NO3}$ is approximately 0.945 in aqueous solution (Table 3). Furthermore, using experimentally-derived molecular vibrations for aqueous NO_2^- and NO_3^- ions yields $^{15}\alpha_{eq,NO2/NO3}$ values of 0.939 (BEGUN and FLETCHER, 1960) or 0.922 (SPINDEL, 1954), which compare favorably to the results presented in Table 3.

The equilibrium fractionation factor for this isotope exchange reaction can be represented by the ratio of kinetic fractionation factors for forward and reverse reactions (O'LEARY, 1981). In this case, the forward and reverse reactions are nitrite oxidation and nitrate reduction, respectively. The kinetic fractionation factor for nitrite oxidation ($^{15}\alpha_{k,NXR}$) can therefore be estimated from the computed equilibrium fractionation factor ($^{15}\alpha_{eq,NO2/NO3}$) and the kinetic fractionation factor for nitrate reduction ($^{15}\alpha_{k,NAR}$):

$$^{15}\alpha_{eq,NO2/NO3} = \left[\frac{^{15}NO_2^- / ^{14}NO_2^-}{^{15}NO_3^- / ^{14}NO_3^-}\right]_{eq} = \frac{^{15}\alpha_{k,NXR}}{^{15}\alpha_{k,NAR}} \quad (5)$$

Each estimate for $^{15}\alpha_{eq,NO2/NO3}$ was less than unity (Table 3), suggesting that $^{15}\alpha_{k,NXR}$ is lower than $^{15}\alpha_{k,NAR}$ and that ^{15}N accumulates preferentially in NO_3^- at equilibrium. Assuming that the fractionation factor for nitrate reduction by the enzyme nitrite oxidoreductase (operating in

512 reverse) is between 1.020 and 1.030, as has been observed for nitrate reductases (Table 1;
513 (BARFORD et al., 1999; DELWICHE and STEYN, 1970; GRANGER et al., 2006), the value of
514 $^{15}\alpha_{k,NXR}$ estimated from equation 5 would vary between 0.964 and 0.973. Because of
515 simplifications made in calculating the equilibrium isotope effects, they should be seen as
516 approximations. However, rather than indicating a role for the reverse reaction in driving an
517 artificial inverse kinetic isotope effect, these calculations suggest that the isotope effect for nitrite
518 oxidation may actually be inverse. In order for the calculated $^{15}\alpha_{eq,NO2/NO3}$ values to be consistent
519 with a normal $^{15}\alpha_{k,NXR}$, $^{15}\alpha_{k,NAR}$ would have to be greater than 1.058, which is unlikely though
520 not impossible (TCHERKEZ and FARQUHAR, 2006).
521 It is interesting that the observed $^{15}\alpha_{k,NXR}$ value of 0.9872 is actually closer to 1 ('more
522 normal') than expected from the results of these calculations. This may reflect partial rate
523 determination by steps prior to nitrite oxidation to nitrate, such as transport into and out of the
524 cell, diffusion to the enzyme active site, or fractionation associated with enzyme/substrate
525 association and dissociation. The expression of enzyme-level isotope effects in the external
526 medium does indeed require exchange of substrates and products between the interior and
527 exterior of the cell (FARQUHAR et al., 1982; GRANGER et al., 2008; NEEDOBA et al., 2004;
528 O'LEARY, 1981). If diffusion or uptake of nitrite is partially rate-limiting, these processes could
529 invalidate the use of a simple unidirectional Rayleigh model to fit the *N. mobilis* data. However,
530 in this case, the observed kinetic isotope effect should provide a minimum estimate of the inverse
531 kinetic isotope effect because the processes of diffusion and transport would be expected to
532 occur with normal isotope effects. There are a series of assumptions that should be tested by
533 experiment, such as the isotope effect for nitrate reduction by nitrite oxidoreductase and the
534 equilibrium fractionation between nitrite and nitrate. However, current calculations suggest that

535 in addition to an inverse kinetic fractionation in the oxidation reaction, any reversibility would
536 tend to further lower the observed kinetic isotope effect.
537 The data from experiments 1-3 were also compared with a simple reaction reversibility
538 model (*Electronic Annex 2*) to determine whether enzyme reversibility was detectable in the
539 culture conditions employed here. Figure 3 shows the simulated $\delta^{15}N_{NO2}$ and $\delta^{15}N_{NO3}$ values for
540 four scenarios with different rates of nitrate reduction, relative to nitrite oxidation. This ratio of
541 forward (nitrite oxidation) and reverse (nitrate reduction) reactions is represented by the
542 parameter $x = {}^{14}k_{NXR}/{}^{14}k_{NAR}$, which is set to values of 0, 0.2, 0.5, and 1.0 in the different
543 simulations. This formulation assumes both nitrite oxidation and nitrate reduction are first order
544 with respect to their substrates.
545 As the amount of reaction reversibility (x) increases from 0 to 1, significant differences are
546 seen in the relationship of $\delta^{15}N_{NO2}$ and $\delta^{15}N_{NO3}$ to the apparent extent of reaction (as determined
547 from $[NO_2^-]$) (Figure 3). With any significant amount of nitrate reduction, the forward reaction
548 fails to go to completion and there is always some NO_2^- that remains in the simulation (Figure
549 EA2.1). This is also indicated by *f* values failing to reach 0 (Figure 3). Nitrate reduction also
550 leads to enhanced separation of ^{15}N between NO_2^- and NO_3^- (Figure 3), and at equilibrium, the
551 remaining NO_2^- would be expected to have a $\delta^{15}N$ value that is approximately 50‰ lower than
552 $\delta^{15}N_{NO3}$. Furthermore, at values of x greater than 0.2, the $\delta^{15}N_{NO2}$ and $\delta^{15}N_{NO3}$ values no longer
553 appear to follow a closed-system "Rayleigh" model. Although $\delta^{15}N_{NO2}$ decreases in all
554 simulations, the behavior of $\delta^{15}N_{NO3}$ changes dramatically. Rather than decreasing towards the
555 initial $\delta^{15}N_{NO2}$ value, $\delta^{15}N_{NO3}$ gradually increases to its equilibrium $\delta^{15}N$ value. This value is
556 based on the concentrations of NO_2^- and NO_3^- that remain in the system at equilibrium and the
557 assumed value of ${}^{15}\alpha_{eq,NO2/NO3}$.

558 Comparison of these results to the *N. mobilis* data from experiments 1-3 suggests that little
559 reversibility occurred (Figure 3). The $\delta^{15}N_{NO2}$ and $\delta^{15}N_{NO3}$ observations fall between the x = 0
560 and x = 0.2, consistent with little or no reversibility in the experiments described here.
561 Furthermore, nitrite concentrations decreased to less than 1% of their initial value in all
562 experiments, suggesting that there was at most 1% reaction reversibility (x = 0.01). At this time,
563 both the current observations and calculations are consistent with little reversibility of nitrite
564 oxidoreductase under near-neutral pH conditions (HOLLOCHER, 1984; STRAAT and NASON, 1965;
565 TANAKA et al., 1983; YAMANAKA and FUKUMORI, 1988).
566
567 *4.1.3. Enzyme-Level Inverse Isotope Effect*
568 Evaluations of both the pre-equilibrium and the enzyme reversibility scenarios imply that the
569 kinetic fractionation factor for nitrite oxidation is likely to be inverse at the enzyme level.
570 Enzyme-level inverse kinetic isotope effects have rarely, if ever, been demonstrated
571 unambiguously in biochemical systems, making the results of the current study both surprising
572 and novel. Several studies have reported apparent inverse kinetic isotope effects but these were
573 shown to result from either pH-dependent pre-equilibrium (FRY et al., 1984), reaction branching
574 (FRY et al., 1985; MCCREADY et al., 1975), or reaction reversibility (WEISS et al., 1988). In one
575 case, the mechanism resulting in the observed inverse kinetic isotope effect was attributed to
576 association and dissociation kinetics of the enzyme and substrate (GAWLITA et al., 1995), while
577 in another case the mechanism was never identified (MCCREADY et al., 1975). However, the
578 current results suggest that an inverse isotope effect is plausible, and even predictable, for the
579 simple N-O bond forming reaction involved in nitrite oxidation. This hypothesis is examined

580 further using transition state theory applied to the current understanding of the mechanism for
581 nitrite oxidation.
582 The reaction mechanism for nitrite oxidation has been studied using oxygen isotope transfer
583 between H_2O, NO_2^-, and NO_3^- species, and the currently accepted reaction mechanism involves a
584 relatively simple oxygen (O) atom addition to NO_2^- (Equation 6). Previous studies have
585 suggested that the reaction proceeds by initial oxygenation of the enzyme's metal cofactor (M)
586 from either NO_3^- or H_2O to form an oxo complex in the +2 oxidation state (M=O). This step is
587 followed by NO_2^- binding to the enzyme-bound O, reduction of the metal cofactor to the +0 state,
588 and dissociation of the produced NO_3^- (DISPIRITO and HOOPER, 1986; FRIEDMAN et al., 1986).
589
590 $$M = O + NO_2^- \longleftrightarrow \left[M - O - NO_2 \right] \longleftrightarrow M + NO_3^- \quad (6)$$
591
592 Using this reaction mechanism as a model, one can predict the isotope effect for nitrite
593 oxidation using transition state theory (TST), which has often been used to describe the kinetics
594 and isotopic fractionation of chemical and biochemical reactions (CLELAND, 1987; NORTHROP,
595 1981; O'LEARY, 1977; THORNTON and THORNTON, 1978). Key assumptions in TST are that the
596 transition state activated complex is in thermal equilibrium with the reactants and that the rate of
597 reaction depends on the transmission coefficient and the concentration of molecules in the
598 activated complex (BIGELEISEN, 1949; BIGELEISEN, 1952; BUDDENBAUM and SHINER, 1977).
599 With these assumptions, the kinetic fractionation factor can be estimated with knowledge of the
600 vibrational frequencies for the substrate and transition state, using equation 7 (BIGELEISEN, 1949;
601 BIGELEISEN and WOLFSBERG, 1958; HUSKEY, 1991):.
602

603 $$\alpha_k = k_1/k_2 = (v'_{1L}/v'_{2L})\left[1 + \sum_i^{3n-6} G(u_i)\Delta u_i - \sum_i^{3n'-6} G(u'_i)\Delta u'_i\right] \quad (7)$$

604

605 In equation 7, u_i is defined as in equation 2, $G(u_i) = [1/2 - (1/u_i) + 1/(e^{ui} - 1)]$., and primed
606 variables refer to properties of the transition state ([M-O-NO_2] in equation 6). The term v'_{1L}/v'_{2L}
607 is the ratio of imaginary frequencies in the transition state along the reaction coordinate for light
608 and heavy molecules, respectively; this term is always greater than 1 (FRY, 1970; SHEPPARD et
609 al., 1954) and can be determined from the reduced masses of the isotopic atoms involved in the
610 bond being formed or broken (SHEPPARD et al., 1954). The term in square brackets, which is
611 based on the zero point energy difference between the substrate and transition state for the light
612 and heavy molecules (BIGELEISEN, 1952), can be greater than or less than 1, depending on the
613 change in the bonding environment at the isotopically substituted atom between substrate and
614 activated complex (SHEPPARD et al., 1954). If N is more strongly bonded in the substrates than in
615 the transition state (a typical bond-breaking reaction), the sum of $G(u_i)\Delta u_i$ for the substrates will
616 be greater than the sum of $G(u_i')\Delta u_i'$ in the transition state and the term in square brackets (eq. 7)
617 will be greater than 1, leading to a normal kinetic isotope effect. This is the case for most
618 nitrogen-oxide reduction reactions (nitrate reduction, nitrite reduction, nitrous oxide reduction),
619 which involve N-O bond breaking (BARFORD et al., 1999; BRYAN et al., 1983; GRANGER et al.,
620 2006). If, however, N is more strongly bonded in the transition state than in the substrates (a
621 bond forming reaction), the sum of $G(u_i)\Delta u_i$ in the reactants will be less than the sum of
622 $G(u_i')\Delta u_i'$ in the transition state, and the term in the square brackets will be less than one. This
623 can lead to an inverse kinetic isotope effect if the product of this term and the imaginary
624 frequency term (v'_{1L}/v'_{2L}) leads to a ratio of rate constants (k_1/k_2) that is less than one. If,

however, the product of the imaginary frequency term and the zero point energy term is greater than 1, a normal kinetic isotope effect would be expected, even for a bond-forming reaction.

Here, the kinetic isotope effect for nitrite oxidation was estimated from equation 7 assuming that the transition state contains the newly formed N-O bond (FRIEDMAN et al., 1986) and that the geometry and bonding environment of the N atom in this complex are similar to nitrate (FRIEDMAN et al., 1986; SHEPPARD et al., 1954). Assuming N-O bonding in the transition state is similar to that of the product (nitrate) may overestimate the bonding difference between the substrate and the transition state. This will be considered in the discussion below. The value of the imaginary frequency term was estimated to be 1.0182, from the square root of the ratio of reduced masses of the bond forming atoms, ^{15}N-^{16}O and ^{14}N-^{16}O (SHEPPARD et al., 1954). The zero point energy terms were estimated from the molecular vibration frequencies of both isotopically substituted forms of NO_2^- (assumed substrate) and NO_3^- (assumed geometry for N in the activated complex). Using both experimental and *ab initio* frequencies for NO_2^- and NO_3^- (Table 2), the ZPE term was estimated to range from 0.933 to 0.941, depending on whether observed or calculated frequencies in aqueous or gas phase are used. Multiplying by the imaginary frequency term, the inherent kinetic isotope effect for nitrite oxidation to nitrate would therefore be predicted from TST (eqn. 7) to be on the order of 0.950-0.958. This $^{15}\alpha_{k,NXR}$ value estimated from TST is lower (more inverse) than was observed experimentally (Figure 2). It is also similar, but a bit lower than the $^{15}\alpha_{k,NXR}$ value predicted from equilibrium calculations (0.964-0.973; section 4.1.2.). However both of these estimates are consistent with the expectation of an inverse kinetic isotope effect for nitrite oxidation.

There are many reasons for the exact values of measured and calculated kinetic isotope effects to differ. Uncertainties involved in estimating $^{15}\alpha_{k,NXR}$ from the equilibrium exchange

reaction for NO_2^- and NO_3^- were discussed above (section 4.1.2). Application of transition state theory also involves inherent assumptions about the enzyme-bound transition state structure and vibrational frequencies, as well as the potential energy surfaces for isotopically substituted molecules (NORTHROP, 1981; THORNTON and THORNTON, 1978). Assuming that the transition state bonding and vibration frequencies are similar to NO_3^- is likely to exaggerate the difference in molecular properties between NO_2^- and the transition state. If the transition state properties are more intermediate between NO_2^- and NO_3^-, the fractionation factor may indeed be closer to 1 (less inverse). Because of this uncertainty, it may not be surprising that the observed fractionation factor is less inverse than the theoretical value calculated from TST.

Even if the estimates of $^{15}\alpha_{k,NXR}$ based on TST provide an accurate estimate for the inherent kinetic isotope effect for nitrite oxidation, it may differ from the isotope effect observed experimentally because of the influence of cellular processes and enzymatic steps prior to the oxidation of nitrite (NORTHROP, 1981; O'LEARY, 1981; TCHERKEZ and FARQUHAR, 2006). Cellular processes that could cause some deviation of the observed isotope effect relative to the predicted (inherent) value cannot currently be ruled out (transport, diffusion, or leakage of NO_2^- from the cell). Indeed, for the enzyme-level kinetic isotope effect to be expressed, some leakage of NO_2^- from the cell must occur. Given that diffusion and transport processes are expected to have normal kinetic isotope effects, these processes could cause some "renormalization" of the observed kinetic isotope effect relative to the theoretical values.

Two of the common causes for apparent inverse isotope fractionation have now been explored: pre-equilibrium (Section 4.1.1.) and enzyme reversibility (Section 4.1.2.), neither of which appear to be the underlying mechanism for inverse kinetic isotope fractionation during nitrite oxidation. Indeed, evaluation of the equilibrium isotope effect for ^{15}N exchange between

671 NO_2^- and NO_3^- suggested that the fractionation factor for nitrite oxidation is likely to be inverse.
672 Evaluation of the fractionation factor using transition state theory provided an independent
673 confirmation of the inverse enzyme-level inverse isotope effect for nitrite oxidoreductase. While
674 there are uncertainties in each of these calculations, the fact that a new N-O bond is being formed
675 without concurrent bond breakage in NO_2^- is a unique aspect of the nitrite oxidation reaction.
676 Overall, the reaction results in increased bonding to the central N atom, and the observed inverse
677 isotope effect suggests that the enzyme-bound transition state contains the new N-O bond.
678

679 **4.2. Implications for Nitrogen Isotope Biogeochemistry**

680 An enzyme-level inverse kinetic isotope effect is unusual in biochemistry. The observation
681 here of a large inverse kinetic isotope effect in the oxidation of nitrite by *N. mobilis* is supported
682 qualitatively by theory, although further work is required to understand whether other cellular
683 processes might mask an even higher inverse kinetic isotope effect. Understanding the cellular
684 controls on the isotope effect for nitrite oxidation will allow us to better predict how the isotope
685 effect for this process is expressed in the environment and how it should be parameterized in
686 ocean biogeochemical models. At this point, it is important to recognize that this process occurs
687 with a fractionation factor that is inverse (less than 1), which challenges the commonly held
688 assumption that all biochemical processes fractionate against the heavier isotope.

689 An inverse isotope effect for nitrite oxidation may help explain the large $\Delta\delta^{15}N$ (= $\delta^{15}N_{NO3}$ -
690 $\delta^{15}N_{NO2}$) values observed in the eastern tropical north Pacific (ETNP), mentioned above. In a
691 previous study, nitrite oxidation was considered as a mechanism for altering the $\delta^{15}N_{NO3}$ and
692 $\delta^{18}O_{NO3}$ profiles, particularly on the upper edge of the suboxic zone, where calculations
693 suggested that nitrite and oxygen may be consumed concurrently (CASCIOTTI and MCILVIN,

694 2007). However, adequate explanations for the low $\delta^{15}N_{NO2}$ values and high $\Delta\delta^{15}N$ values were
695 not found, holding to constraints of a 25‰ isotope effect for nitrate reduction ($^{15}\varepsilon_{k,NAR}$ =
696 ($^{15}\alpha_{k,NAR}$-1)*1000) and either a 'normal' or non-fractionating nitrite consumption process. For
697 example, nitrite reduction with a normal isotope effect ($^{15}\varepsilon_{k,NIR}$) of +15‰ (BRYAN et al., 1983;
698 CASCIOTTI, 2002; CASCIOTTI et al., 2002) would tend to cause isotopic enrichment in the NO_2^-
699 pool, counteracting the isotopic depletion of the nitrite pool generated by nitrate reduction. At
700 steady state, that is for nitrite concentrations and $\delta^{15}N_{NO2}$ values not changing (or changing
701 slowly relative to the production and consumption fluxes), the $\Delta\delta^{15}N$ value would tend towards
702 $^{15}\varepsilon_{k,NAR}$ - $^{15}\varepsilon_{k,NIR}$, or 25‰ – 15‰ = 10‰. The observed $\Delta\delta^{15}N$ values of 28-35‰ are therefore
703 difficult to explain with nitrite reduction as the sole sink for nitrite. Non steady-state conditions
704 between nitrite production and consumption processes may contribute to $\Delta\delta^{15}N$ values greater
705 than 25‰, but are unlikely to explain the low $\delta^{15}N_{NO2}$ values.
706 If nitrite oxidation by marine NOB routinely occurs with an inverse kinetic isotope effect, as
707 observed here for *N. mobilis*, then nitrite oxidation would tend to lower $\delta^{15}N_{NO2}$ values and
708 enhance the ^{15}N depletion of NO_2^- achieved by nitrate reduction. A simple steady-state box
709 model including the fluxes of nitrite reduction (F_{NIR}), nitrite oxidation (F_{NXR}), and nitrate
710 reduction ($F_{NAR} = F_{NIR} + F_{NXR}$), was used to estimate the dependence of $\Delta\delta^{15}N$ on F_{NXR}/F_{NAR}.
711
712 $$\Delta\delta^{15}N = {}^{15}\varepsilon_{k,NAR} - {}^{15}\varepsilon_{k,NXR} * F_{NXR}/F_{NAR} - {}^{15}\varepsilon_{k,NIR} * F_{NIR}/F_{NAR} \quad (8)$$
713
714 Equation 8 predicts that $\Delta\delta^{15}N$ values should increase as nitrite oxidation becomes a greater
715 fraction of the nitrite consumption flux. Figure 4 shows the steady state $\delta^{15}N_{NO2}$, $\delta^{15}N_{NO3}$, and
716 $\Delta\delta^{15}N$ values obtained from this exercise, as well as the relationship between $\Delta\delta^{15}N$ and

717 F_{NXR}/F_{NAR} (inset). For these calculations, $^{15}\varepsilon_{k,NAR}$ was assumed to be +25‰, $^{15}\varepsilon_{k,NXR}$ = -13‰,
718 and $^{15}\varepsilon_{k,NIR}$ = +15‰. Data from the ETNP are overlaid on $\Delta\delta^{15}N$ contours in Figure 4,
719 illustrating the high $\Delta\delta^{15}N$ values and low $\delta^{15}N_{NO2}$ values observed in the ETNP suboxic zone
720 (CASCIOTTI and MCILVIN, 2007). The data from the ETNP oxygen minimum zone suggest that
721 nitrite oxidation may be an important sink for NO_2^- in this region ($\Delta\delta^{15}N$ > 28‰, F_{NXR}/F_{NAR}
722 >0.7) (Figure 4). This is consistent with previous interpretations based on Δ(15,18) (CASCIOTTI
723 and MCILVIN, 2007).
724 More generally, the opposing isotope effects for nitrite oxidation and reduction processes
725 suggest that $\Delta\delta^{15}N$ might be used to distinguish between oxidative and reductive fates for nitrite.
726 Where reductive fates for nitrite dominate over oxidative fates ($F_{NIR} < 0.5 * F_{NAR}$), $\Delta\delta^{15}N$ would
727 be expected to be less than the isotope effect for nitrate reduction to nitrite in a given setting
728 (approximately 25‰ in suboxic zones, or 5‰ in the euphotic zone) (Equation 8). Conversely,
729 where the consumption of nitrite through oxidation exceeds the flux of nitrite consumed by
730 reductive processes ($F_{NXR} > 0.5 * F_{NAR}$), $\Delta\delta^{15}N$ would be expected to be greater than the isotope
731 effect for nitrate reduction (Equation 8). These isotope effects are most likely to be observed in
732 or near ocean suboxic zones with high concentrations of NO_2^-. However, the isotope effect for
733 nitrite oxidation may also be expressed in the euphotic zone or in the primary nitrite maximum at
734 the base of the euphotic zone, where competing fates for nitrite may lead to branching between
735 nitrite assimilation into particulate nitrogen and nitrite oxidation to nitrate.
736
737 **4.3. Future Work**
738 It will be important to expand these observations beyond *N. mobilis* to examine the generality
739 of these results among nitrite oxidizing microorganisms and to obtain comparable data on $\delta^{18}O$

fractionation by nitrite-oxidizing bacteria. There are 4 known genera of nitrite oxidizing bacteria, which differ from each other in many ways: *Nitrococcus*, *Nitrobacter*, *Nitrospira*, and *Nitrospina*, and it will be important to determine whether the inverse isotope effect is universal among different species and growth conditions.

Examination of the $\delta^{18}O$ fractionation factor during nitrite oxidation holds promise for independently verifying the conclusions from the current study based on $\delta^{15}N$. For example, these additional measurements have the power to independently verify the reversibility of the reaction, the structure of the transition state, and the reaction mechanism. At the same time, interpreting the $\delta^{18}O$ data is more complex because of the analytical challenges posed by abiotic equilibration of oxygen atoms between nitrite and water (CASCIOTTI et al., 2007), as well as the potential for biochemical exchange of nitrite with water catalyzed by the bacteria themselves (DISPIRITO and HOOPER, 1986; FRIEDMAN et al., 1986; HOLLOCHER, 1984). Further work is required to fully resolve the effects of oxygen isotope equilibration from the interpretation of the kinetic isotope effect for oxygen isotopes, since in some situations equilibration will act in the same direction to lower $\delta^{18}O_{NO2}$, and in other cases it will have counteracting effects on $\delta^{18}O_{NO2}$.

It is also important to examine the kinetic isotope effects with isolated nitrite oxidoreductase enzyme to resolve the contribution of complicating factors, such as NO_2^- transport and diffusion, to the observed enzyme-level kinetic isotope effect. Nitrite oxidoreductase remains active in cell extracts (TANAKA et al., 1983; YAMANAKA and FUKUMORI, 1988) and can be partially purified for use in these experiments.

Acknowledgements. The author would like to acknowledge stimulating conversations with John Hayes and Carolyn Buchwald during the preparation of this manuscript. Comments on an earlier

763 draft were provided by Julie Granger, Tom Trull, and by the author's lab group: Carolyn
764 Buchwald, Dan Rogers, Erin Banning, Matthew McIlvin, Edward Leadbetter, and Caitlin Frame.
765 Excellent technical assistance was also provided by Matthew McIlvin. Funding from NSF award
766 OCE 05-26277 to KLC is also gratefully acknowledged.
767
768

TABLES

TABLE 1: Nitrogen isotope effects for microbial processes in pure culture

Process	Reaction	$^{15}\alpha_k = {}^{14}k/{}^{15}k$	$^{15}\varepsilon_k$ (‰) $= (^{15}\alpha_k - 1)\times 10^3$	References
Nitrate reduction (Denitrification)	$NO_3^- \rightarrow NO_2^-$	1.013 to 1.030	+13‰ to +30‰	BARFORD et al., 1999; DELWICHE and STEYN, 1970; GRANGER et al., 2006
Nitrite reduction (Denitrification)	$NO_2^- \rightarrow NO$	1.005 to 1.025	+5‰ to +25‰	BRYAN et al., 1983
Nitrous oxide reduction (Denitrification)	$N_2O \rightarrow N_2$	1.004 to 1.013	+4‰ to +13‰	BARFORD et al., 1999; OSTROM et al., 2007
Nitrate reduction (Nitrate assimilation)	$NO_3^- \rightarrow NO_2^-$	1.005 to 1.010	+5‰ to +10‰	GRANGER et al., 2004; NEEDOBA and HARRISON, 2004; WASER et al., 1998a
Nitrogen fixation	$N_2 \rightarrow N_{org}$	0.998 to 1.002	-2‰ to +2‰	DELWICHE and STEYN, 1970; HOERING and FORD, 1960; MEADOR et al., 2007
Ammonium assimilation	$NH_4^+ \rightarrow N_{org}$	1.014-1.027	+14‰ to +27‰	HOCH et al., 1992; WASER et al., 1998a
Ammonia oxidation* (Nitrification)	$NH_4^+ \rightarrow NO_2^-$	1.014 to 1.038	+14‰ to +38‰	CASCIOTTI et al., 2003; MARIOTTI et al., 1981; YOSHIDA, 1988; DELWICHE AND STEYN, 1970
Nitrite oxidation (Nitrification)	$NO_2^- \rightarrow NO_3^-$	0.9872	-12.8‰	This study

* $^{15}\alpha_k$ for ammonia oxidation is reported relative to NH_4^+, which is not the substrate for ammonia oxidation. Instead, the observed $^{15}\alpha_k$ relative to NH_4^+ should be corrected for NH_4^+/NH_3 equilibrium fractionation, dividing the observed $^{15}\alpha_k$ by a correction factor of 1.0183 at pH 8 (WEISS et al., 1988), which yields isotope effects of 0.996 to 1.0194 for ammonia oxidation relative to NH_3.

774 **TABLE 2**: Molecular vibration frequencies used to calculate isotope exchange equilibria.

	[1]Aqueous phase *ab initio* calculations ω_t (cm^{-1})		[2]Gas phase *ab initio* calculations ω_t (cm^{-1})		[3]Aqueous and [4]gas phase observations ω_t (cm^{-1})	
	^{14}N	^{15}N	^{14}N	^{15}N	^{14}N	^{15}N
NO_2^-	795.770	790.733	792.684	787.911	808	805
	1316.199	1288.788	1338.523	1310.613	1232	1208
	1386.788	1362.958	1377.186	1353.122	1326	1305
	This study		This study		[3]BEGUN and FLETCHER, 1960	
NO_3^-	708.514	706.678	706.396	704.737	716.8	714.8
	708.800	706.953	706.518	704.865	716.8	714.8
	829.003	807.405	837.870	816.030	830.9	809.0
	1089.308	1089.308	1077.496	1077.496	1049.2	1049.2
	1438.454	1404.619	1471.120	1436.134	1375.6	1343.7
	1438.681	1404.820	1471.151	1436.177	1375.6	1343.7
	This study		This study		[3]BEGUN and FLETCHER, 1960	
HNO_2 (trans)	596.345	595.140	600.998	599.845	543.880	542.90
	671.375	668.799	630.216	627.954	595.620	593.20
	906.346	886.079	863.359	844.223	790.118	773.62
	1308.670	1308.112	1325.358	1324.390	1263.183	1262.45
	1731.762	1700.779	1794.972	1762.652	1699.800	1669.60
	3210.523	3210.478	3698.573	3698.576	3590.711	N/D
	This study		This study		[4]DEELEY and MILLS, 1985	

775

776 [1]Calculated in the WebMO interface using Gaussian, B3LYP, 'routine', in aqueous solution.

777 [2]Calculated in the WebMO interface using Gaussian, B3LYP, 'routine', in gas phase.

778 [3]Observed in aqueous solution (BEGUN and FLETCHER, 1960).

779 [4]Observed in gas phase as trans-HONO (DEELEY and MILLS, 1985).

780

780 **TABLE 3**: Calculated isotope exchange equilibria

	Medium	$^{15}\alpha_{eq}$ [1]
HNO_2/NO_2^-	aqueous	0.9975
	gas phase	0.9972
NO_2^-/NO_3^-	aqueous	0.9454
	gas phase	0.9418

781

782 [1]Calculated from the ratios of Q_2/Q_1 using equations 2 and 3 at T = 298 K and *ab initio* frequencies from Table 2.

783

784

784 **REFERENCES**
785

786 Ahlers, B., Konig, W., and Bock, E., 1990. Nitrite reductase activity in *Nitrogacter vulgaris*.
787 *FEMS Microbiology Letters* **67**, 121-126.
788 Altabet, M. A., 2007. Constraints on oceanic N balance/imbalance from sedimentary ^{15}N records.
789 *Biogeosciences* **4**, 75-86.
790 Anbar, A. D., Jarzecki, A. A., and Spiro, T. G., 2005. Theoretical investigation of iron isotope
791 fractionation between $Fe(H_2O)_6^{3+}$ and $Fe(H_2O)_6^{2+}$: Implications for iron stable isotope
792 geochemistry. *Geochimica et Cosmochimica Acta* **69**, 825-837.
793 Anderson, J. J., Okubo, A., Robbins, A. S., and Richards, F. A., 1982. A model for nitrite and
794 nitrate distributions in oceanic oxygen minimum zones. *Deep-Sea Research* **29**, 1113-
795 1140.
796 Barford, C. C., Montoya, J. P., Altabet, M. A., and Mitchell, R., 1999. Steady-state Nitrogen
797 isotope effects of N_2 and N_2O production in *Paracoccus denitrificans*. *Applied and*
798 *Environmental Microbiology* **65**, 989-994.
799 Bartosch, S., Wolgst, I., Speick, E., and Bock, E., 1999. Identification of nitrite-oxidizing
800 bacteria with monoclonal antibodies recognizing the nitrite oxidoreductase. *Applied and*
801 *Environmental Microbiology* **65**, 4162-4133.
802 Begun, G. M. and Fletcher, W. H., 1960. Partition function ratios for molecules containing
803 nitrogen isotopes. *The Journal of Chemical Physics* **33**, 1083-1085.
804 Bigeleisen, J., 1949. The relative reaction velocities of isotopic molecules. *The Journal of*
805 *Chemical Physics* **17**, 675-678.
806 Bigeleisen, J., 1952. The effects of isotopic substitution on the rates of chemical reactions.
807 *Canadian Journal of Chemistry*, 823-828.
808 Bigeleisen, J., 1965. Chemistry of Isotopes. *Science* **147**, 463-471.
809 Bigeleisen, J. and Mayer, M. G., 1947. Calculation of Equilibrium Constants for Isotopic
810 Exchange Reactions. *Journal of Chemical Physics* **15**, 261-267.
811 Bigeleisen, J. and Wolfsberg, M., 1958. Theoretical and experimental aspects of isotope effects
812 in chemical kinetics. *Advances in Chemical Physics* **1**, 15-76.
813 Bock, E., Wilderer, P. A., and Freitag, A., 1988. Growth of *Nitrobacter* in the absence of
814 dissolved oxygen. *Water Research* **22**, 245-250.
815 Böhlke, J. K., Mroczkowski, S. J., and Coplen, T. B., 2003. Oxygen isotopes in nitrate: new
816 reference materials for O-18 : O-17 : O-16 measurements and observations on nitrate-
817 water equilibration. *Rapid Communications in Mass Spectrometry* **17**, 1835-1846.
818 Boon, B. and Laudelout, H., 1962. Kinetics of Nitrite Oxidation by *Nitrobacter winogradskyi*.
819 *Biochemical Journal* **85**, 440-447.
820 Brandes, J. A. and Devol, A. H., 2002. A global marine fixed nitrogen isotopic budget:
821 Implications for Holocene nitrogen cycling. *Global Biogeochemical Cycles* **16**, 1120.
822 Brandes, J. A., Devol, A. H., Yoshinari, T., Jayakumar, D. A., and Naqvi, S. W. A., 1998.
823 Isotopic composition of nitrate in the central Arabian Sea and eastern tropical North
824 Pacific: a tracer for mixing and nitrogen cycles. *Limnology and Oceanography* **43**, 1680-
825 1689.
826 Bryan, B. A., Shearer, G., Skeeters, J. L., and Kohl, D. H., 1983. Variable Expression of the
827 Nitrogen Isotope Effect Associated With Denitrification of Nitrite. *Journal of Biological*
828 *Chemistry* **258**, 8613-8617.

829 Buddenbaum, W. E. and Shiner, V. J., 1977. Computation of Isotope Effects on Equilibria and
830 Rates. In: Cleland, O'Leary, and Northrop (Eds.), *Isotope Effects on Enzyme-Catalyzed*
831 *Reactions*. University Park Press, Baltimore.
832 Casciotti, K. L., 2002. Molecular and stable isotopic characterization of enzymes involved in
833 nitrification and nitrifier-denitrification., Princeton University.
834 Casciotti, K. L., Böhlke, J. K., McIlvin, M. R., Mroczkowski, S. J., and Hannon, J. E., 2007.
835 Oxygen Isotopes in Nitrite: Analysis, Calibration, and Equilibration. *Analytical*
836 *Chemistry* **79**, 2427-2436.
837 Casciotti, K. L. and McIlvin, M. R., 2007. Isotopic analyses of nitrate and nitrite from reference
838 mixtures and application to Eastern Tropical North Pacific waters. *Marine Chemistry*
839 **107**, 184-201.
840 Casciotti, K. L., Sigman, D. M., Galanter Hastings, M., Böhlke, J. K., and Hilkert, A., 2002.
841 Measurement of the oxygen isotopic composition of nitrate in seawater and freshwater
842 using the denitrifier method. *Analytical Chemistry* **74**, 4905-4912.
843 Casciotti, K. L., Sigman, D. M., and Ward, B. B., 2003. Linking diversity and stable isotope
844 fractionation in ammonia-oxidizing bacteria. *Geomicrobiology Journal* **20**, 335-353.
845 Cleland, W. W., 1987. The Use of Isotope Effects in the Detailed Analysis of Catalytic
846 Mechanisms of Enzymes. *Bioinorganic Chemistry* **15**, 283-302.
847 Cline, J. D. and Kaplan, I. R., 1975. Isotopic fractionation of dissolved nitrate during
848 denitrification in the Eastern Tropical North Pacific Ocean. *Mar. Chem.* **3**, 271-299.
849 Codispoti, L. A. and Christensen, J. P., 1985. Nitrification, denitrification, and nitrous oxide
850 cycling in the eastern tropical Pacific Ocean. *Marine Chemistry* **16**, 277-300.
851 Codispoti, L. A., Friederich, G. E., Packard, T. T., Glover, H. E., Kelly, P. J., Spinrad, R. W.,
852 Barber, R. T., Elkins, J. W., Ward, B. B., Lipschultz, F., and Lostaunau, N., 1986. High
853 Nitrite Levels Off Northern Peru - a Signal of Instability in the Marine Denitrification
854 Rate. *Science* **233**, 1200-1202.
855 Codispoti, L. A. and Richards, F. A., 1976. An analysis of the horizontal regime of
856 denitrification in the eastern tropical North Pacific. *Limnology and Oceanography* **21**,
857 379-388.
858 Dalsgaard, T., Canfield, D. E., Petersen, J., Thamdrup, B., and Acuna-Gonzalez, J., 2003. N_2
859 production by the anammox reaction in the anoxic water column of Golfo Dulce, Costa
860 Rica. *Nature* **422**, 606-608.
861 Dalsgaard, T., Thamdrup, B., and Canfield, D. E., 2005. Anaerobic ammonium oxidation
862 (anammox) in the marine environment. *Research in Microbiology* **156**, 457-464.
863 Deeley, C. M. and Mills, I. M., 1985. Nitrous acid: vibrational frequency shifts due to ^{15}N
864 substitution, and the harmonic force field. *Molecular Physics* **54**, 23-32.
865 Delwiche, C. C. and Steyn, P. L., 1970. Nitrogen isotope fractionation in soils and microbial
866 reactions. *Environmental Science and Technology* **4**, 929-935.
867 Deutsch, C., Sigman, D. M., Thunell, R. C., Meckler, A. N., and Haug, G. H., 2004. Isotopic
868 constraints on glacial/interglacial changes in the oceanic nitrogen budget. *Global*
869 *Biogeochemical Cycles* **18**.
870 Devol, A. H., Uhlenhopp, A. G., Naqvi, S. W. A., Brandes, J. A., Jayakumar, D. A., Nakamura,
871 K., Gaurin, S., Codispoti, L. A., and Yoshinari, T., 2006. Denitrification rates and excess
872 nitrogen gas concentrations in the Arabian Sea oxygen deficient zone. *Deep-Sea*
873 *Research I* **53**, 1533-1547.

874 DiSpirito, A. A. and Hooper, A. B., 1986. Oxygen Exchange between Nitrate Molecules during
875 Nitrite Oxidation by *Nitrobacter*. *The Journal of Biological Chemistry* **261**, 10534-
876 10537.
877 Farquhar, G. D., Oleary, M. H., and Berry, J. A., 1982. On the Relationship Between Carbon
878 Isotope Discrimination and the Inter-Cellular Carbon-Dioxide Concentration in Leaves.
879 *Australian Journal of Plant Physiology* **9**, 121-137.
880 Francis, C. A., Beman, J. M., and Kuypers, M. M. M., 2007. New processes and players in the
881 nitrogen cycle: the microbial ecology of anaerobic and archaeal ammonia oxidation. *Isme*
882 *Journal* **1**, 19-27.
883 Freitag, A. and Bock, E., 1990. Energy conservation in *Nitrobacter*. *FEMS Microbiology Letters*
884 **66**, 157-162.
885 Freitag, A., Rudert, M., and Bock, E., 1987. Growth of *Nitrobacter* by dissimilatory nitrate
886 reduction. *FEMS Microbiology Letters* **48**, 105-109.
887 Friedman, S. H., Massefski, W., and Hollocher, T. C., 1986. Catalysis of Intermolecular Oxygen
888 Atom Transfer By Nitrite Dehydrogenase of *Nitrobacter agilis*. *Journal of Biological*
889 *Chemistry* **261**, 10538-10543.
890 Fry, A., 1970. Heavy Atom Isotope Effects in Organic Reaction Mechanism Studies. In: Collins
891 and Bowman (Eds.), *Isotope Effects in Chemical Reactions*. Van Nostrand Reinhold,
892 New York.
893 Fry, B., Gest, H., and Hayes, J. M., 1984. Isotope effects associated with the anaerobic oxidation
894 of sulfide by the purple photosynthetic bacterium, *Chromatium vinosum*. *FEMS*
895 *Microbiology Letters* **22**, 283-287.
896 Fry, B., Gest, H., and Hayes, J. M., 1985. Isotope effects associated with the anaerobic oxidation
897 of sulfite and thiosulfite by the photosynthetic bacterium, *Chromatium vinosum*. *FEMS*
898 *Microbiology Letters* **27**, 227-232.
899 Gawlita, E., Caldwell, W. S., Oleary, M. H., Paneth, P., and Anderson, V. E., 1995. Kinetic
900 Isotope Effects On Substrate Association - Reactions of Phosphoenolpyruvate With
901 Phosphoenolpyruvate Carboxylase and Pyruvate-Kinase. *Biochemistry* **34**, 2577-2583.
902 Granger, J., Sigman, D. M., Lehman, M. F., and Tortell, P. D., 2008. Nitrogen and oxygen
903 isotope fractionation during dissimilatory nitrate reduction by denitrifying bacteria.
904 *Limnology and Oceanography* **53**, 2533-2545.
905 Granger, J., Sigman, D. M., Needoba, J. A., and Harrison, P. J., 2004. Coupled nitrogen and
906 oxygen isotope fractionation of nitrate during assimilation by cultures of marine
907 phytoplankton. *Limnology and Oceanography* **49**, 1763-1773.
908 Granger, J., Sigman, D. M., Prokopenko, M. G., Lehman, M. F., and Tortell, P. D., 2006. A
909 method for nitrite removal in nitrate N and O isotope analyses. *Limnology and*
910 *Oceanography: Methods* **4**, 205-212.
911 Hamersley, M. R., Lavik, G., Woebken, D., Rattray, J. E., Lam, P., Hopmans, E. C., Sinninghe
912 Damste, J. S., Kruger, S., Graco, M., Gutierrez, D., and Kuypers, M. M. M., 2007.
913 Anaerobic ammonium oxidation in the Peruvian oxygen minimum zone. *Limnology and*
914 *Oceanography* **52**, 923-933.
915 Hoch, M. P., Fogel, M. L., and Kirchman, D. L., 1992. Isotope Fractionation Associated With
916 Ammonium Uptake By a Marine Bacterium. *Limnology and Oceanography* **37**, 1447-
917 1459.
918 Hoering, T. and Ford, H. T., 1960. The isotope effect in the fixation of nitrogen by *Azotobacter*.
919 *J. Amer. Chem. Soc.* **82**, 376-378.

Hollocher, T. C., 1984. Source of the Oxygen Atoms of Nitrate in the Oxidation of Nitrite by *Nitrobacter agilis* and Evidence Against a P-O-N Anhydride Mechanism in Oxidative-Phosphorylation. *Archives of Biochemistry and Biophysics* **233**, 721-727.

Huskey, W. P., 1991. Origins and Interpretations of Heavy-Atom Isotope Effects. In: Cook, P. F. (Ed.), *Enzyme Mechanisms from Isotope Effects*. CRC Press, Boca Raton, FL.

Kumar, S. and Nicholas, D. J. D., 1982. Assimilation of Inorganic Nitrogen Compounds by *Nitrobacter agilis*. *Journal of General Microbiology* **128**, 1795-1801.

Kuypers, M. M. M., Lavik, G., Woebken, D., Schmid, M., Fuchs, B. M., Amann, R., Jorgensen, B. B., and Jetten, M. S. M., 2005. Massive nitrogen loss from the Benguela upwelling system through anaerobic ammonium oxidation. *Proceedings of the National Academy of Sciences of the United States of America* **102**, 6478-6483.

Kuypers, M. M. M., Sliekers, A. O., Lavik, G., Schmid, M., Jorgensen, B. B., Kuenen, J. G., Sinninghe Damste, J. S., Strous, M., and Jetten, M. S. M., 2003. Anaerobic ammonium oxidtaion by anammox bacteria in the Black Sea. *Nature* **422**, 608-611.

Lipschultz, F., Wofsy, S. C., Ward, B. B., Codispoti, L. A., Friedrich, G., and Elkins, J. W., 1990. Bacterial Transformations of Inorganic Nitrogen in the Oxygen- Deficient Waters of the Eastern Tropical South-Pacific Ocean. *Deep-Sea Research Part A-Oceanographic Research Papers* **37**, 1513-1541.

Mariotti, A., Germon, J. C., Hubert, P., Kaiser, P., Letolle, R., Tardieux, A., and Tardieux, P., 1981. Experimental determination of nitrogen kinetic isotope fractionation: some principles; Illustration for the denitrification and nitrification processes. *Plant and Soil* **62**, 413-430.

McCready, R. G. L., Laishley, E. J., and Krouse, H. R., 1975. Stable isotope fractionation by *Clostridium pasteurianum*. 1. $^{34}S/^{32}S$: inverse isotope effects during SO_4^{2-} and SO_3^{2-} reduction. *Canadian Journal of Microbiology* **21**, 235-244.

McIlvin, M. R. and Altabet, M. A., 2005. Chemical conversion of nitrate and nitrite to nitrous oxide for nitrogen and oxygen isotopic analysis in freshwater and seawater. *Analytical Chemistry* **77**, 5589-5595.

Meador, T. B., Aluwihare, L. I., and Mahaffey, C., 2007. Isotopic heterogeneity and cycling of organic nitrogen in the oligotrophic ocean. *Limnology and Oceanography* **52**, 934-947.

Meincke, M., Bock, E., Kastrau, D., and Kroneck, P. M. H., 1992. Nitrite oxidoreductase from *Nitrobacter hamburgensis*: redox centers and their catalytic role. *Archives of Microbiology* **158**, 127-131.

Needoba, J. A. and Harrison, P. J., 2004. Influence of low light and a light/dark cycle on NO_3^- uptake, intracellular NO_3^-, and nitrogen isotope fractionation by marine phytoplankton. *Journal of Phycology* **40**, 505-516.

Needoba, J. A., Sigman, D. M., and Harrison, P. J., 2004. The mechanism of isotope fractionation during algal nitrate assimilation as illuminated by the N-15/N-14 of intracellular nitrate. *Journal of Phycology* **40**, 517-522.

Northrop, D. B., 1981. The Expression of Isotope Effecs on Enzyme-Catalyzed Reactions. *Annual Reviews of Biochemistry* **50**, 103-131.

O'Leary, M. H., 1977. Studies of Enzyme Reaction Mechanisms by Means of Heavy-atom Isotope Effects. In: Cleland, O'Leary, and Northrop (Eds.), *Isotope Effects on Enzyme-Catalyzed Reactions*. University Park Press, Baltimore.

O'Leary, M. H., 1981. Carbon isotope fractionations in plants. *Phytochemistry* **20**, 553-567.

Ostrom, N. E., Pitt, A., Sutka, R., Ostrom, P. H., Grandy, A. S., Huizinga, K. M., and Robertson, G. P., 2007. Isotopologue effects during N_2O reduction in soils and in pure cultures of denitrifiers. *Journal of Geophysical Research* **112**, G02005.

Richet, P., Bottinga, Y., and Javoy, M., 1977. A review of hydrogen, carbon, nitrogen, oxygen, sulfur, and chlorine stable isotope fractionation among gaseous molecules. *Annual Reviews of Earth and Planetary Science* **5**, 65-110.

Riordan, E., Minogue, N., Healy, D., O'Driscoll, P., and Sodeau, J. R., 2005. Spectroscopic and Optimization Modeling Study of Nitrous Acid in Aqueous Solution. *Journal of Physical Chemistry A* **109**, 779-786.

Schauble, E. A., Rossman, G. R., and Taylor, H. P., 2001. Theoretical estimates of equilibrium Fe-isotope fractionations from vibrational spectroscopy. *Geochimica et Cosmochimica Acta* **65**, 2487-2497.

Scott, K. M., Lu, X., Cavanaugh, C. M., and Liu, J. S., 2004. Optimal methods for extimating kinetic isotope effects from different forms of the Rayleigh distillation equation. *Geochimica et Cosmochimica Acta* **68**, 433-442.

Sheppard, W. A., Bader, R. F. W., and Bourns, A. N., 1954. Sulfur isotope effects in the bisulfite addition reaction of aldehydes and ketones. II. Bond-formation effect. *Canadian Journal of Chemistry* **32**, 345-350.

Sigman, D. M., Casciotti, K. L., Andreani, M., Barford, C., Galanter, M., and Böhlke, J. K., 2001. A bacterial method for the nitrogen isotopic analysis of nitrate in seawater and freshwater. *Analytical Chemistry* **73**, 4145-4153.

Sigman, D. M., Granger, J., DiFiore, P. J., Lehmann, M. F., Ho, R., Cane, G., and van Geen, A., 2005. Coupled nitrogen and oxygen isotope measurements of nitrate along the eastern North Pacific margin. *Global Biogeochemical Cycles* **19**, GB4022.

Sigman, D. M., Robinson, R., Knapp, A. N., van Geen, A., McCorkle, D. C., Brandes, J. A., and Thunell, R. C., 2003. Distinguishing between water column and sedimentary denitrification in the Santa Barbara Basin using the stable isotopes of nitrate. *Geochemistry Geophysics Geosystems* **4**.

Spieck, E. and Bock, E., 2001. The nitrite-oxidizing bacteria. In: Garrity, G. M., Stanley, T. W., Staley, J. T., Brenner, D. J., Holt, J. G., Boone, D. R., Castenholz, R. W., Krieg, N. R., and Schleifer, H.-H. (Eds.), *Bergey's manual of systematic bacteriology*. Williams and Wilkins Co., Baltimore, MD.

Spindel, W., 1954. The Calculation of Equilibrium Constants for Several Eschange Reactions of Nitrogen-15 between Oxy Compounds of Nitrogen. *Journal of Chemical Physics* **22**, 1271-1272.

Starkenburg, S. R., Chain, P. S. G., Sayavedra-Soto, L. A., Hauser, L., Land, M. L., Larimer, F. W., Malfatti, S. A., Klotz, M. G., Bottomley, P. J., Arp, D. J., and Hickey, W. J., 2006. Genome Sequence of the Chemolithoautotrophic Nitrite-Oxidizing Bacterium *Nitrobacter winogradskyi* Nb-255. *Applied and Environmental Microbiology* **72**, 2050-2063.

Starkenburg, S. R., Larimer, F. W., Stein, L. Y., Klotz, M. G., Chain, P. S. G., Sayavedra-Soto, L. A., Poret-Peterson, A. T., Gentry, M. E., Arp, D. J., Ward, B., and Bottomley, P. J., 2008. Complete Genome Sequence of *Nitrobacter hamburgensis* X14 and Comparative Genomic Sequence Analysis of Species within the Genus *Nitrobacter*. *Applied and Environmental Microbiology* **74**, 2852-2863.

Straat, P. A. and Nason, A., 1965. Characterization of a Nitrate Reductase from the Chemoautotroph *Nitrobacter agilis*. *The Journal of Biological Chemistry* **240**, 1412-1426.

Strickland, J. D. H. and Parsons, T. R., 1972. A practical handbook of seawater analysis, 2nd ed. *Bull. Fish. Res. Bd. Canada* **167**, 1-310.

Sundermeyer-Klinger, H., Meyer, W., Warninghoff, B., and Bock, E., 1984. Membrane-Bound Nitrite Oxidoreductase of *Nitrobacter*: Evidence For a Nitrate Reductase System. *Archives of Microbiology* **140**, 153-158.

Tanaka, Y., Fukumori, Y., and Yamanaka, T., 1983. Purification of cytochrome a_1c_1 from *Nitrobacter agilis* and characterization of nitrite oxidation system of the bacterium. *Archives of Microbiology* **135**, 265-271.

Tcherkez, G. and Farquhar, G. D., 2006. Isotopic fractionation by plant nitrate reductase, twenty years later. *Functional Plant Biology* **33**, 531-537.

Thornton, E. K. and Thornton, E. R., 1978. Scope and Limitations of the Concept of the Transition State. In: Gandour and Schowen (Eds.), *Transition States of Biochemical Processes*. Plenum Press, New York.

Urey, H. C., 1947. The Thermodynamic Properties of Isotopic Substances. *Journal of the Chemical Society*, 562-581.

Voss, M., Dippner, J. W., and Montoya, J. P., 2001. Nitrogen isotope patterns in the oxygen-deficient waters of the Eastern Tropical North Pacific Ocean. *Deep-Sea Research Part I-Oceanographic Research Papers* **48**, 1905-1921.

Ward, B. B., Glover, H. E., and Lipschultz, F., 1989. Chemoautotrophic activity and nitrification in the oxygen minimum zone off Peru. *Deep-Sea Research* **36**, 1031-1051.

Waser, N. A., Yin, K. D., Yu, Z. M., Tada, K., Harrison, P. J., Turpin, D. H., and Calvert, S. E., 1998a. Nitrogen isotope fractionation during nitrate, ammonium and urea uptake by marine diatoms and coccolithophores under various conditions of N availability. *Marine Ecology-Progress Series* **169**, 29-41.

Waser, N. A. D., Turpin, D. H., Harrison, P. J., Nielsen, B., and Calvert, S. E., 1998b. Nitrogen isotope fractionation during the uptake and assimilation of nitrate, nitrite, and urea by a marine diatom. *Limnology and Oceanography* **43**, 215-224.

Watson, S. W. and Waterbury, J. B., 1971. Characteristics of two marine nitrite oxidizing bacteria, *Nitrospina gracilis* nov. gen. nov. sp. and *Nitrococcus mobilis* nov. gen. Nov. sp. *Archives of Microbiology* **77**, 203-230.

Weiss, P. M., Chen, C.-Y., Cleland, W. W., and Cook, P. F., 1988. Use of primary deuterium and 15N isotope effects to deduce the relative rates of steps in the mechanisms of alanine and glutamate dehydrogenases. *Biochemistry* **27**, 4814-4822.

Yamanaka, T., 1996. Mechanisms of Oxidiation of Inorganic Electron Donors in Autotrophic Bacteria. *Plant Cell Physiology* **37**, 569-574.

Yamanaka, T. and Fukumori, Y., 1988. The Nitrite Oxidizing System of *Nitrobacter winogradskyi*. *FEMS Microbiology Reviews* **54**, 259-270.

Yoshida, N., 1988. ^{15}N-depleted N_2O as product of nitrification. *Nature* **355**, 528-529.

FIGURE 1: Time course results from *N. mobilis* experiments1, 2, and 3.

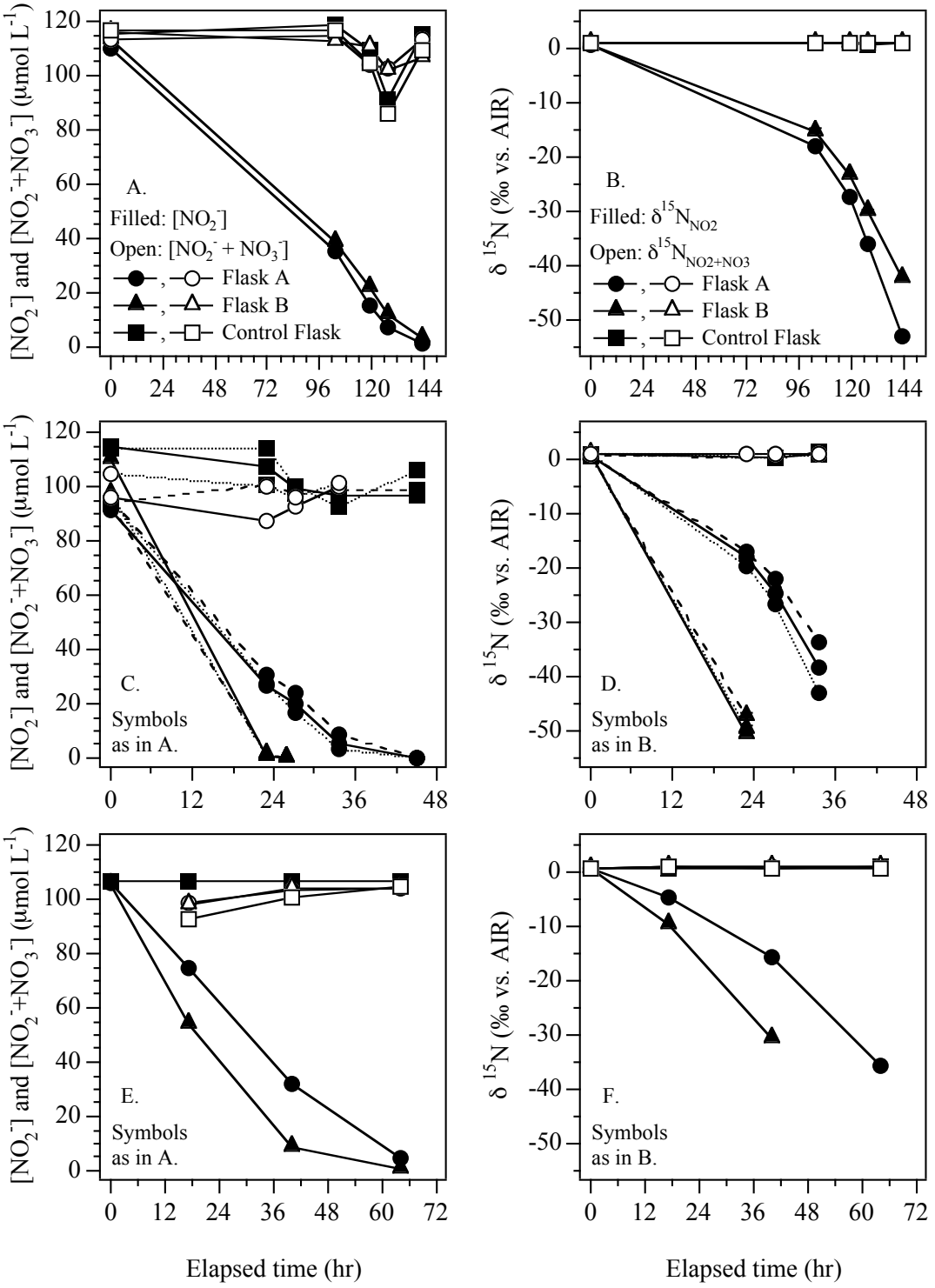

Figure 1. $[NO_2^-]$ (filled symbols) and $[NO_2^- + NO_3^-]$ (open symbols) are shown for time course experiments 1 (panel A), 2 (panel C), and 3 (Panel E). Please note the use of different x-axes for experiments 1, 2, and 3. $\delta^{15}N_{NO2}$ (filled symbols) and $\delta^{15}N_{NO2+NO3}$ (open symbols) are shown for the same experiments in panels B, D, and F, respectively. In every panel circles represent data from flask A, triangles represent data from flask B, and squares denote data from the control flask. In experiment 2 (panels C and D), there were triplicate A, B, and control flasks, denoted by unique line dashing (solid, dotted, dashed) for replicate flasks. Error bars for $\delta^{15}N_{NO2}$ and $\delta^{15}N_{NO2+NO3}$ are smaller than the symbols.

FIGURE 2: Rayleigh plot of nitrite $\delta^{15}N$ from *N. mobilis* experiments 1, 2, and 3.

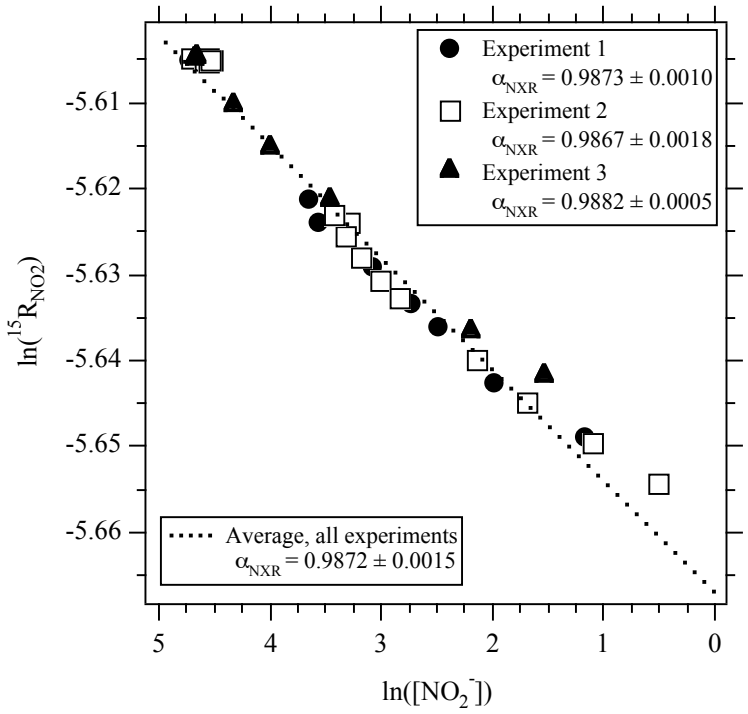

Figure 2. Rayleigh plot for nitrite oxidation, using $\ln(^{15}R_{NO2})$ vs. $\ln([NO_2^-])$, for experiments 1 (filled circles), 2 (open squares), and 3 (filled triangles). The fractionation factor for nitrite oxidation ($^{15}\alpha_{k,NXR}$) estimated using dummy variables and averaging over all three experiments was 0.9872 ± 0.0015. For reference, the fractionation line $^{15}\alpha_{k,NXR}$ = 0.9872 is shown (dotted line). Error bars are smaller than the data points.

FIGURE 3: Modeled effect of enzyme reversibility on expression of KIE

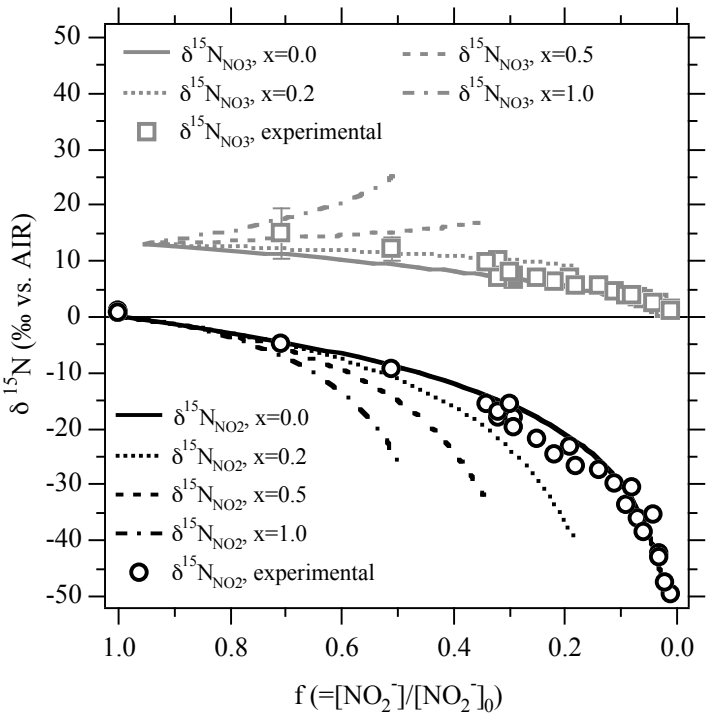

Figure 3. Model simulations for enzyme-level reversibility of nitrite oxidoreductase. Simulated $\delta^{15}N_{NO2}$ (black lines) and $\delta^{15}N_{NO3}$ (grey lines) are plotted versus *f* (=$[NO_2^-]/[NO_2^-]_0$) for varying amounts of back-reaction (x = $^{14}k_{NAR}/^{14}k_{NXR}$; see *Electronic Supplement 2* for model details). Line dashing denotes simulations with a specified amount of back-reaction: x = 0.0 (solid lines), x = 0.2 (dotted lines), x = 0.5 (dashed lines), and x = 1.0 (dot-dashed lines). Overlain in each panel are experimental observations for $\delta^{15}N_{NO2}$ (open black circles) and $\delta^{15}N_{NO3}$ (open grey squares) from experiments 1, 2, and 3 (see text). Error bars for $\delta^{15}N_{NO2}$ measurements are smaller than the symbols. Experimental data are consistent with very low ($0.0 \leq x \leq 0.2$) amounts of back-reaction.

FIGURE 4: Expression of Inverse KIE in $\Delta\delta^{15}N$

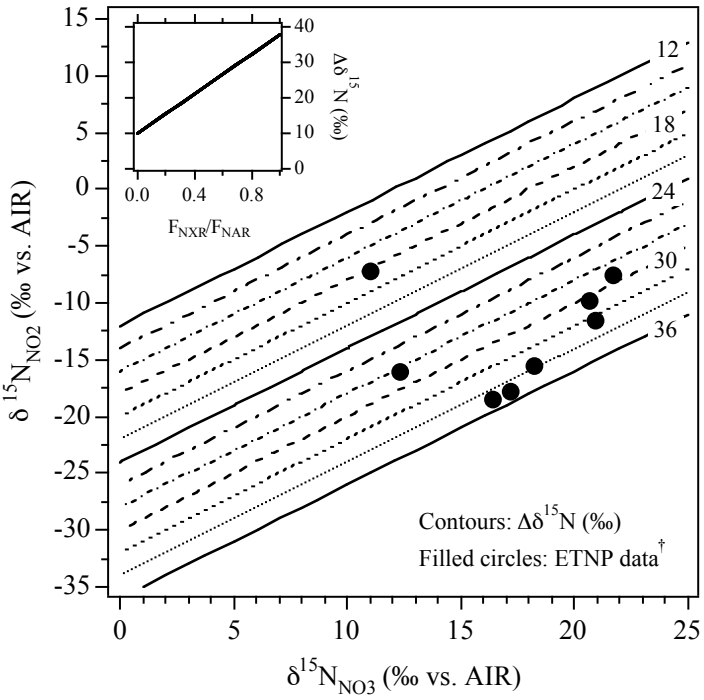

Figure 4. Contour plot of simulated suboxic zone $\delta^{15}N_{NO2}$ (‰ vs. AIR), $\delta^{15}N_{NO3}$ (‰ vs. AIR), and $\Delta\delta^{15}N$ (= $\delta^{15}N_{NO3}$-$\delta^{15}N_{NO2}$) for varying F_{NXR}/F_{NAR}. Assumptions for the simulation include: $^{15}\varepsilon_{k,NAR}$ = +25‰, $^{15}\varepsilon_{k,NXR}$ = -12.8‰, and $^{15}\varepsilon_{k,NIR}$ = +15‰, with nitrite concentration and $\delta^{15}N_{NO2}$ held in steady state (see text/supplement for details). Contouring denotes 2‰ increments of $\Delta\delta^{15}N$ (‰) with a range of 12-36‰. Overlaid on the contour plot are observations from the Eastern Tropical North Pacific (ETNP) (black circles; †Casciotti and McIlvin, 2007). Inset plot shows the dependence of $\Delta\delta^{15}N$ (‰) on F_{NXR}/F_{NAR} in the simulation. ETNP data show $\Delta\delta^{15}N$ values of 18-36‰, corresponding to simulated F_{NXR}/F_{NAR} values of 0.3-0.9.

CASCIOTTI (W5860) ELECTRONIC ANNEX 1

EA.1. Simulations for Pre-equilibrium Scenarios

In order to illustrate the role of a pre-equilibrium between HNO_2 and NO_2^- on the expressed kinetic isotope effect for nitrite oxidation, six different closed-system simulations were conducted with different assumptions for $^{15}\alpha_{eq,HNO2/NO2}$, $^{15}\alpha_{k,NXR}$, and enzyme substrate (Table EA1.1).

Table EA1.1. Adjustable parameters for pre-equilibrium simulations.

Simulation	Substrate	$^{15}\alpha_{eq,HNO2/NO2}$	$^{15}\alpha_{k,NXR}$
S1	HNO_2	1.0280	1.0150
S2	NO_2^-	1.0280	1.0150
S3	HNO_2	0.9972	1.0150
S4	NO_2^-	0.9972	1.0150
S5	HNO_2	0.9972	0.9872
S6	NO_2^-	0.9972	0.9872

In each simulation, the reaction was taken to be first order in substrate concentration. It was also assumed that isotope exchange equilibration between HNO_2 and NO_2^- was rapid relative to the rate of oxidation, and that the oxidation reaction itself was irreversible. For simulations 1, 3, and 5 where HNO_2 was taken to be the substrate for oxidation, the following finite-difference equations were used:

$$[^{14}N_T] = [^{14}NO_3^-] + [^{14}NO_2^-] + [H^{14}NO_2] \quad \text{(EA1.1)}$$

$$[^{14}NO_3^-]_t = [^{14}NO_3^-]_{t-1} + {}^{14}k_{NXR} \cdot [H^{14}NO_2]_{t-1} \cdot dt \quad \text{(EA1.2)}$$

$$[^{14}NO_2^-]_t = ([^{14}N_T]_t - [^{14}NO_3^-]_t)/(1+10^{pKa-pH}) \quad \text{(EA1.3)}$$

$$[H^{14}NO_2]_t = ([^{14}N_T]_t - [^{14}NO_3^-]_t) \cdot (10^{pKa-pH})/(1+10^{pKa-pH}) \quad \text{(EA1.4)}$$

$$[^{15}N_T] = [^{15}NO_3^-] + [^{15}NO_2^-] + [H^{15}NO_2] = \text{constant} \quad \text{(EA1.5)}$$

$$[^{15}NO_3^-]_t = [^{15}NO_3^-]_{t-1} + ({}^{14}k_{NXR}/{}^{15}a_{k,NXR}) \cdot [H^{15}NO_2]_{t-1} \cdot dt \quad \text{(EA1.6)}$$

$$[^{15}NO_2^-]_t = ([^{15}N_T]_t - [^{15}NO_3^-]_t)/(1+{}^{15}\alpha_{eq,HNO2/NO2} \cdot [H^{14}NO_2]_t/[^{14}NO_2^-]_t) \quad \text{(EA1.7)}$$

$$[H^{15}NO_2]_t = {}^{15}\alpha_{eq,HNO2/NO2} \cdot [H^{14}NO_2]_t \cdot [^{15}NO_2^-]_t/[^{14}NO_2^-]_t \quad \text{(EA1.8)}$$

For simulations 2, 4, and 6 where NO_2^- was taken to be the substrate for oxidation, the following finite-difference equations were used:

$$[^{14}NO_3^-]_t = [^{14}NO_3^-]_{t-1} + {}^{14}k_{NXR} \cdot [^{14}NO_2]_{t-1} \cdot dt \quad \text{(EA1.9)}$$

$$[^{15}NO_3^-]_t = [^{15}NO_3^-]_{t-1} + ({}^{14}k_{NXR}/{}^{15}a_{k,NXR}) \cdot [^{15}NO_2]_{t-1} \cdot dt \quad \text{(EA1.10)}$$

Equations for $[^{14}N_T]$, $[^{15}N_T]$, $[^{14}NO_2^-]_t$, $[^{15}NO_2^-]_t$, $[H^{14}NO_2]_t$, and $[H^{15}NO_2]_t$ were the same as in simulations 1, 3, and 5 (above).

The simulated $\delta^{15}N$ of NO_2^-, HNO_2, and NO_3^- are plotted versus simulated f ($=[NO_2^-]/[NO_2^-]_0$) in Figure EA1.1. The $\delta^{15}N_{NO2}$ and $\delta^{15}N_{NO3}$ data collected from experiments 1-3 are overlaid on the simulated $\delta^{15}N_{NO2}$ and $\delta^{15}N_{NO3}$ in each panel. Simulations 1, 2, 3, and 4 were all conducted with a normal ${}^{15}\alpha_{k,NXR}$ acting on either HNO_2 (S1, Figure EA1.1A; S3, Figure EA1.1C) or NO_2^- (S2, Figure EA1.1B; S4, Figure EA1.1D) as the substrate. Of these first four simulations, only S1 fit the observed data. These results illustrate that in order for the observed $\delta^{15}N_{NO2}$ and $\delta^{15}N_{NO3}$ data to be explained using a normal kinetic isotope effect, HNO_2 (the minor pool) must be the substrate for the reaction, it must be enriched in ^{15}N relative to the bulk pool, and the equilibrium isotope effect must be about 13‰ higher than the kinetic isotope effect (in this case ${}^{15}\alpha_{eq,HNO2/NO2} = 1.0280$ and ${}^{15}\alpha_{k,NXR} = 1.0150$; Table EA1.1). For example, S1 appears to explain the observations with HNO_2 as the substrate, whereas S2 does not fit the observations with identical fractionation factors, but with the enzyme acting on NO_2^- as the substrate rather than HNO_2. However, in order to fit the observations in S1 using a normal kinetic isotope effect, ${}^{15}\alpha_{eq,HNO2/NO2}$ was set to 1.028. As discussed in the main text, however, our best estimate for the

equilibrium fractionation factor is estimated to be small (0.9975-0.9978), and HNO_2 is expected to be depleted in ^{15}N relative to NO_2^-. Therefore, S1 and S2 can be eliminated.

Constraining $^{15}\alpha_{eq,HNO2/NO2}$ to 0.9975 in S3-S6 illustrates that an inverse kinetic isotope effect for either HNO_2 (S5, Figure EA1.1E) or NO_2^- (S6, Figure EA1.1F) oxidation is required to explain the observations. A normal kinetic isotope effect for either HNO_2 (S3, Figure EA1.1C) or NO_2^- (S4; Figure EA1.1D) cannot explain the observations.

FIGURE EA1.1: Simulated effects of HNO_2/NO_2^- pre-equilibrium on expression of $^{15}\alpha_{k,NXR}$.

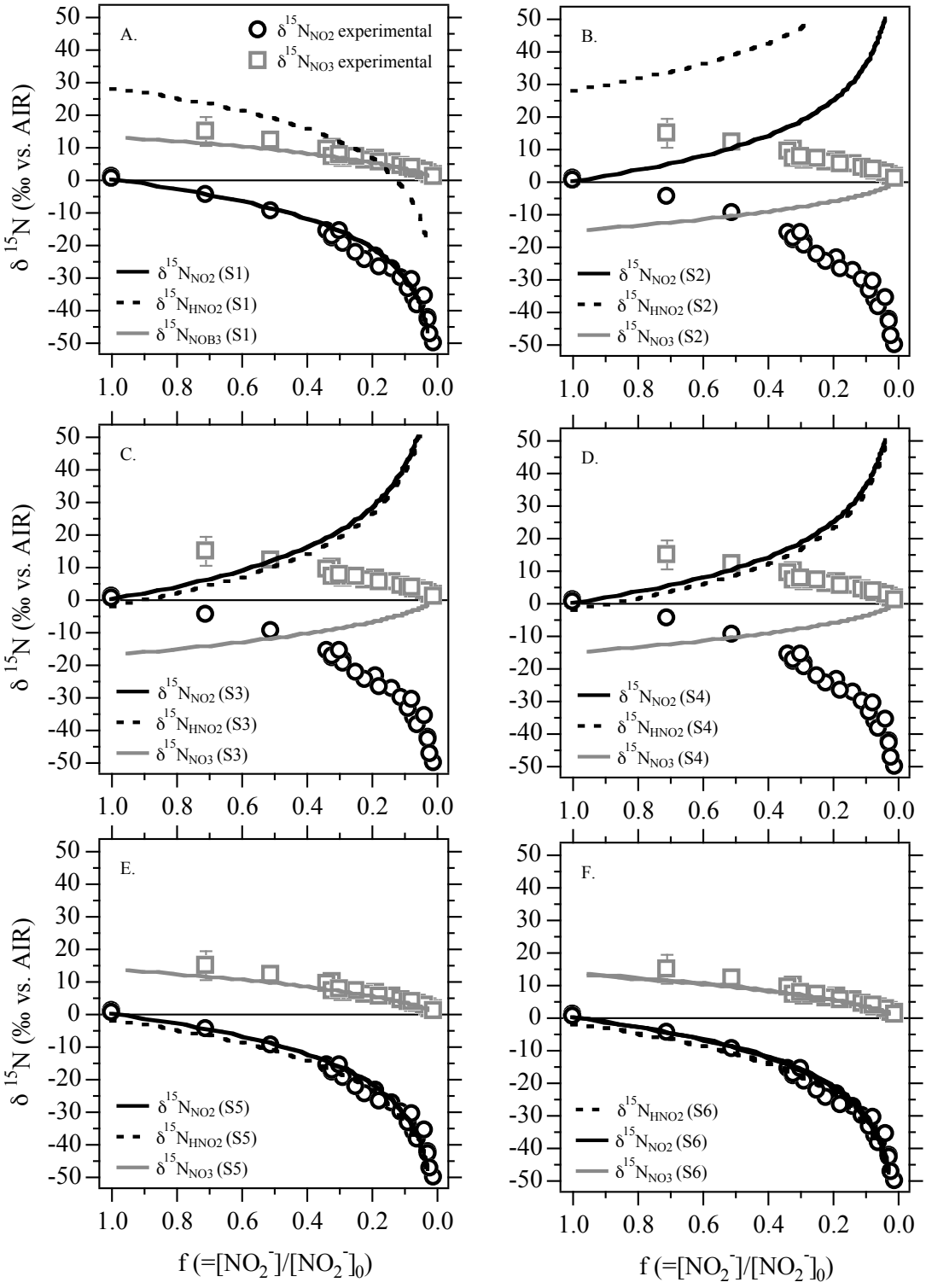

FIGURE EA1.1 LEGEND. Simulated effects of HNO_2/NO_2^- pre-equilibrium on expression of $^{15}\alpha_{k,NXR}$. The different simulations were carried out using equations EA1.1-EA1.10 and the adjustable parameters (substrates, kinetic and equilibrium isotope effects) given in Table EA1.1. Simulated $\delta^{15}N_{NO2}$ (solid black line), $\delta^{15}N_{HNO2}$ (dashed black line), and $\delta^{15}N_{NO3}$ (solid grey line) are plotted versus simulated f ($=[NO_2^-]/[NO_2^-]_0$), with pH held constant at 8.2. Overlaid in each panel are experimental observations for $\delta^{15}N_{NO2}$ (open black circles) and $\delta^{15}N_{NO3}$ (open grey squares) vs. f from experiments 1, 2, and 3 (see main text). Error bars for $\delta^{15}N_{NO3}$ are shown, and for $\delta^{15}N_{NO2}$ are smaller than the symbols.

CASCIOTTI (W5860) ELECTRONIC ANNEX 2

EA2. Model Formulation for Enzyme Reversibility

Reaction reversibility would be expected to affect the time course of $\delta^{15}N_{NO2}$ and $\delta^{15}N_{NO3}$ values and their relationship to $[NO_2^-]$ and $[NO_3^-]$. As noted in the main text, increased reaction reversibility would be expected to lead to the expression of lower (more inverse) $^{15}\alpha_{k,NXR}$ values. Therefore, it is important to know whether nitrate reduction is occurring simultaneously with nitrite oxidation in order to best interpret the results of the current study. To first order, reversibility can be evaluated in the nitrite oxidation/nitrate reduction system through mass and isotope balance calculations. Here, a simple finite difference model was used to examine the effects of reaction reversibility on observed $[NO_2^-]$, $[NO_3^-]$, $\delta^{15}N_{NO2}$, and $\delta^{15}N_{NO3}$. The results from the model are then compared with the experimental results to evaluate evidence for reaction reversibility in the current experiments.

The following equations comprise the model formulation:

$$[^{14}NO_2^-]_t = [^{14}NO_2^-]_{t-1} + {}^{14}k_{NAR} \cdot [^{14}NO_3^-]_{t-1} \cdot dt - {}^{14}k_{NXR} \cdot [^{14}NO_2^-]_{t-1} \cdot dt \quad \text{(EA2.1)}$$

$$[^{14}NO_3^-]_t = [^{14}NO_3^-]_{t-1} - {}^{14}k_{NAR} \cdot [^{14}NO_3^-]_{t-1} \cdot dt + {}^{14}k_{NXR} \cdot [^{14}NO_2^-]_{t-1} \cdot dt \quad \text{(EA2.2)}$$

$$[^{15}NO_2^-]_t = [^{15}NO_2^-]_{t-1} + {}^{15}k_{NAR} \cdot [^{15}NO_3^-]_{t-1} \cdot dt - {}^{15}k_{NXR} \cdot [^{15}NO_2^-]_{t-1} \cdot dt \quad \text{(EA2.3)}$$

$$[^{15}NO_3^-]_t = [^{15}NO_3^-]_{t-1} - {}^{15}k_{NAR} \cdot [^{15}NO_3^-]_{t-1} \cdot dt + {}^{15}k_{NXR} \cdot [^{15}NO_2^-]_{t-1} \cdot dt \quad \text{(EA2.4)}$$

$$^{15}\alpha_{k,NXR} = {}^{14}k_{NXR} / {}^{15}k_{NXR} \quad \text{(EA2.5)}$$

$$^{15}\alpha_{k,NAR} = {}^{14}k_{NAR} / {}^{15}k_{NAR} \quad \text{(EA2.6)}$$

$$^{14}k_{NAR} = x \cdot {}^{14}k_{NXR} \quad \text{(EA2.7)}$$

$$^{15}k_{NAR} = x \cdot {}^{15}k_{NXR} \cdot {}^{15}\alpha_{k,NXR} / {}^{15}\alpha_{k,NAR} \quad \text{(EA2.8)}$$

$$\delta^{15}N_{NO2}\ (‰) = (([^{15}NO_2^-]_t/[^{14}NO_2^-]_t \div {}^{15}R_{AIR}) - 1) \cdot 1000 \quad \text{(EA2.9)}$$

$$\delta^{15}N_{NO3}\ (‰) = (([^{15}NO_3^-]_t/[^{14}NO_3^-]_t \div {}^{15}R_{AIR}) - 1) \cdot 1000 \quad \text{(EA2.10)}$$

In these equations, the molar concentrations (moles L^{-1}) of NO_2^- and NO_3^- containing ^{14}N and ^{15}N are given in brackets, t represents time, dt represents the time step for integration, k's represent first order rate constants (with the dimension t^{-1}) for nitrite oxidation (subscript 'NXR') and nitrate reduction (subscript 'NAR') for ^{14}N-containing molecules (superscript '14') and ^{15}N-containing molecules (superscript '15'). The factor 'x' (dimensionless) represents the ratio of reverse and forward rate constants for ^{14}N-containing molecules. $^{15}\alpha_{k,NXR}$ is taken to be 0.983 and $^{15}\alpha_{k,NAR}$ is taken to be 1.040 so that $^{15}\alpha_{eq,NOx}$ ($=^{15}\alpha_{k,NXR}$ /$^{15}\alpha_{k,NAR}$) is 0.945, as discussed in the main text. Initial conditions were taken to be $[^{14}NO_2^-]_0 = 99.6337 \times 10^{-6}$ moles L^{-1}, $[^{15}NO_2^-]_0 = 0.3663 \times 10^{-6}$ moles L^{-1} and $[^{14}NO_3^-]_0 = [^{15}NO_3^-]_0 = 0 \times 10^{-6}$ moles L^{-1}.

Four time course 'experiments' were run in MS Excel over 70 time steps (with dt = 1), for x equal to 0, 0.2, 0.5 or 1 (Figure EA2.1). In each case with non-zero reversibility (x>0), initial rates of net nitrite oxidation decreased over time, as the reaction came to equilibrium and the mass fluxes through the forward and reverse reaction became balanced (Figure EA2.1A). Increasing reversibility also lowers the initial net rate of nitrite oxidation and the apparent extent of nitrite oxidation, with correspondingly less nitrate accumulation. The only scenario in which nitrite is completely consumed is with no back reaction (x=0).

In each model run, $\delta^{15}N_{NO2}$ decreased over time as expected with the inverse isotope effect (Figure EA2.1B). Increasing amounts of nitrate reduction caused $\delta^{15}N_{NO2}$ to decrease more quickly for a given amount of nitrite oxidation. From the perspective of $\delta^{15}N_{NO2}$, increasing reversibility lead to an increasingly inverse apparent isotope effect (Figure EA2.1C), and the extent of back reaction was difficult to diagnose from $\delta^{15}N_{NO2}$ alone. However, reaction reversibility also led to unique trends in $\delta^{15}N_{NO3}$ over time that should allow us to distinguish between a large irreversible isotope effect and a contribution from enzyme reversibility.

At low values of x, $\delta^{15}N_{NO3}$ decreased over time as it was dominated by the inverse isotope effect for nitrite oxidation (Figure EA2.1B, x = 0, x = 0.2). As the value of x was increased to 0.5, $\delta^{15}N_{NO3}$ remained relatively constant over the time course (Figure EA2.1B), and in the most extreme case (x=1), $\delta^{15}N_{NO3}$ actually increased over time as it approached equilibrium with NO_2^- (Figure EA2.1B). When x was greater than 0.5, the isotope effect for nitrite oxidation based on $\delta^{15}N_{NO3}$ switched from inverse to apparently normal (Figure EA2.1C) while $\delta^{15}N_{NO2}$ fractionation continued to become increasingly inverse. The differential behavior of $\delta^{15}N_{NO2}$ and $\delta^{15}N_{NO3}$ under different levels of reaction reversibility present a diagnostic pattern for reversibility in the $\delta^{15}N_{NO2}/\delta^{15}N_{NO3}$ system, with apparent isotope effects based on $\delta^{15}N_{NO2}$ and $\delta^{15}N_{NO3}$ diverging as the amount of back reaction increases (Figure EA2.1C).

In experiments with *Nitrococcus mobilis*, discussed in the main text, nitrite was completely oxidized to nitrate over the time course experiments (Figure 1). Both nitrite and nitrate become depleted in ^{15}N over time (Figure 1), with $\delta^{15}N_{NO3}$ approaching the initial $\delta^{15}N_{NO2}$ after all of the nitrite had been oxidized to nitrate. The Rayleigh plots were also consistent with a mass balance between NO_2^- and NO_3^- and a nearly irreversible reaction of NO_2^- to NO_3^- under our experimental conditions (Figure 2). Therefore, both the mass and isotope balance observed in *N. mobilis* experiments suggest that reaction reversibility was insignificant under the conditions employed.

FIGURE EA2.1: Reversibility of Nitrite Oxidoreductase

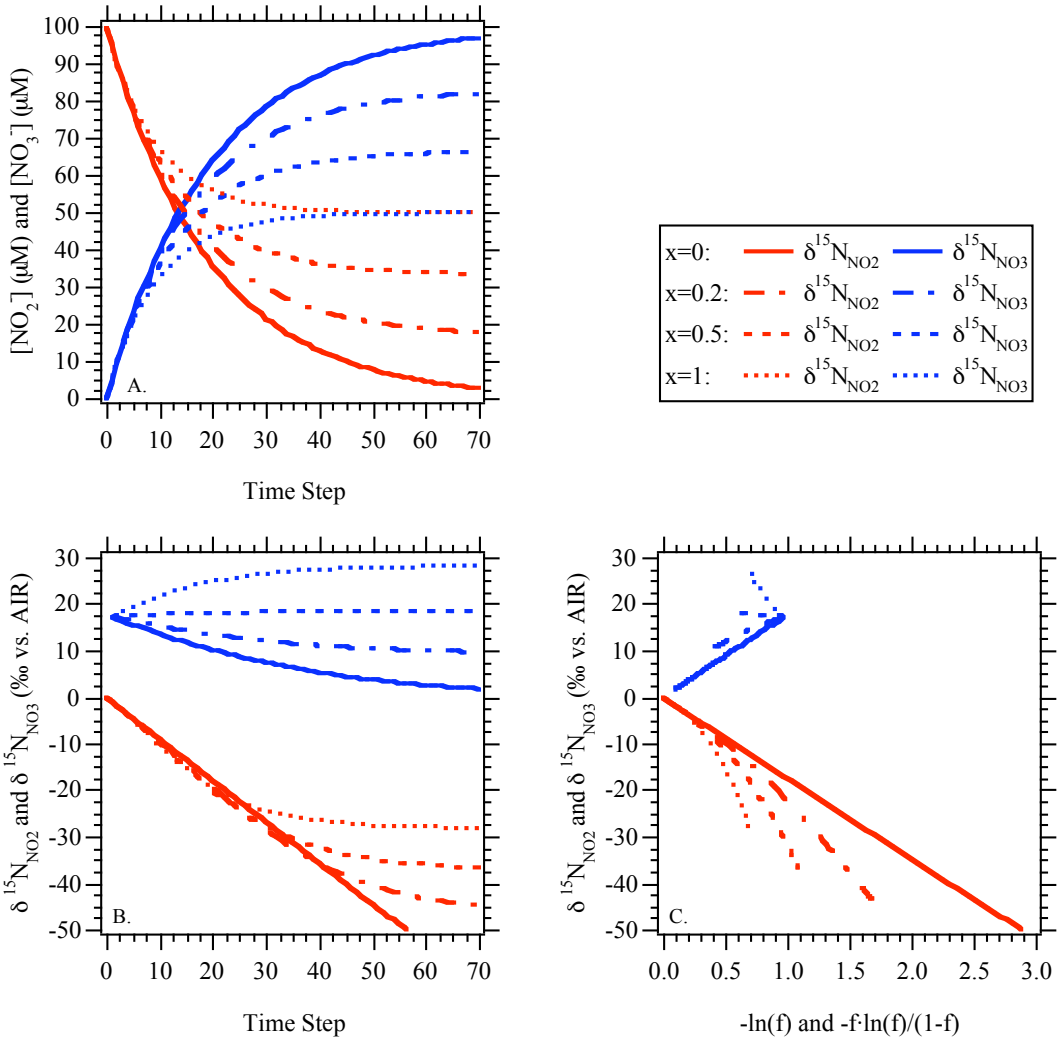

FIGURE EA2.1. Results from nitrite oxidoreductase reversibility model. (A) Modeled nitrite (red) and nitrate (blue) concentrations versus time for x ($=^{14}k_{NAR}/^{14}k_{NXR}$) values of 0, 0.2, 0.5, and 1.0. (B) Modeled $\delta^{15}N_{NO2}$ (red) and $\delta^{15}N_{NO3}$ (blue) versus time for the same values of x. (C) Modeled $\delta^{15}N_{NO2}$ (red) and $\delta^{15}N_{NO3}$ (blue) versus $-\ln(f)$ and $-f\cdot\ln(f)/(1-f$, respectively. In each panel, x = 0 is indicated by the solid line, x = 0.2 by the dot-dashed line, x = 0.5 by the dashed line, and x = 1 by the dotted line.